The Levantine Intermediate Water Experiment (LIWEX) Group: Levantine basin—A laboratory for multiple water mass formation processes

The LIWEX Group[1]

[1] In winter 1995 the last major field work of the Physical Oceanography of the Eastern Mediterranean (POEM) program was carried out, the Levantine Intermediate Water Experiment (LIWEX). In this study a thorough analysis is presented of the data set collected during three successive surveys in January, February, and March–April 1995. The major overall result is that the Levantine basin is shown to be the site for multiple, and different, water mass formation processes. Levantine Deep Water (LDW) was formed in the Rhodes gyre, with the preconditioning phase starting in December 1994. In late January the chimney was ventilating to the atmosphere. In February the strong mixing phase is documented by the convective cell vertically homogeneous to 900 m depth. In March–April, recapping has occurred in the upper 200 m. LDW remained confined inside the Rhodes gyre cyclonic circulation. Levantine Intermediate Water (LIW) is instead deeply affected by the upper thermocline circulation. Shallow ventilating chimneys with the LIW thermostads were found in the January survey inside the cyclonic region of the northern Levantine. The formation process of LIW does not involve deep penetrative convection. Winter surface cooling and evaporation are sufficient to produce a surface mixed layer 100 m deep with LIW characteristics. At the mixed layer basis, LIW subducts and spreads along isopycnal surfaces along pathways determined by the cyclonic/anticyclonic structures of the upper thermocline circulation. *INDEX TERMS:* 4243 Oceanography: General: Marginal and semienclosed seas; 4283 Oceanography: General: Water masses; 4536 Oceanography: Physical: Hydrography; 4223 Oceanography: General: Descriptive and regional oceanography; *KEYWORDS:* water masses, hydrography, marginal seas
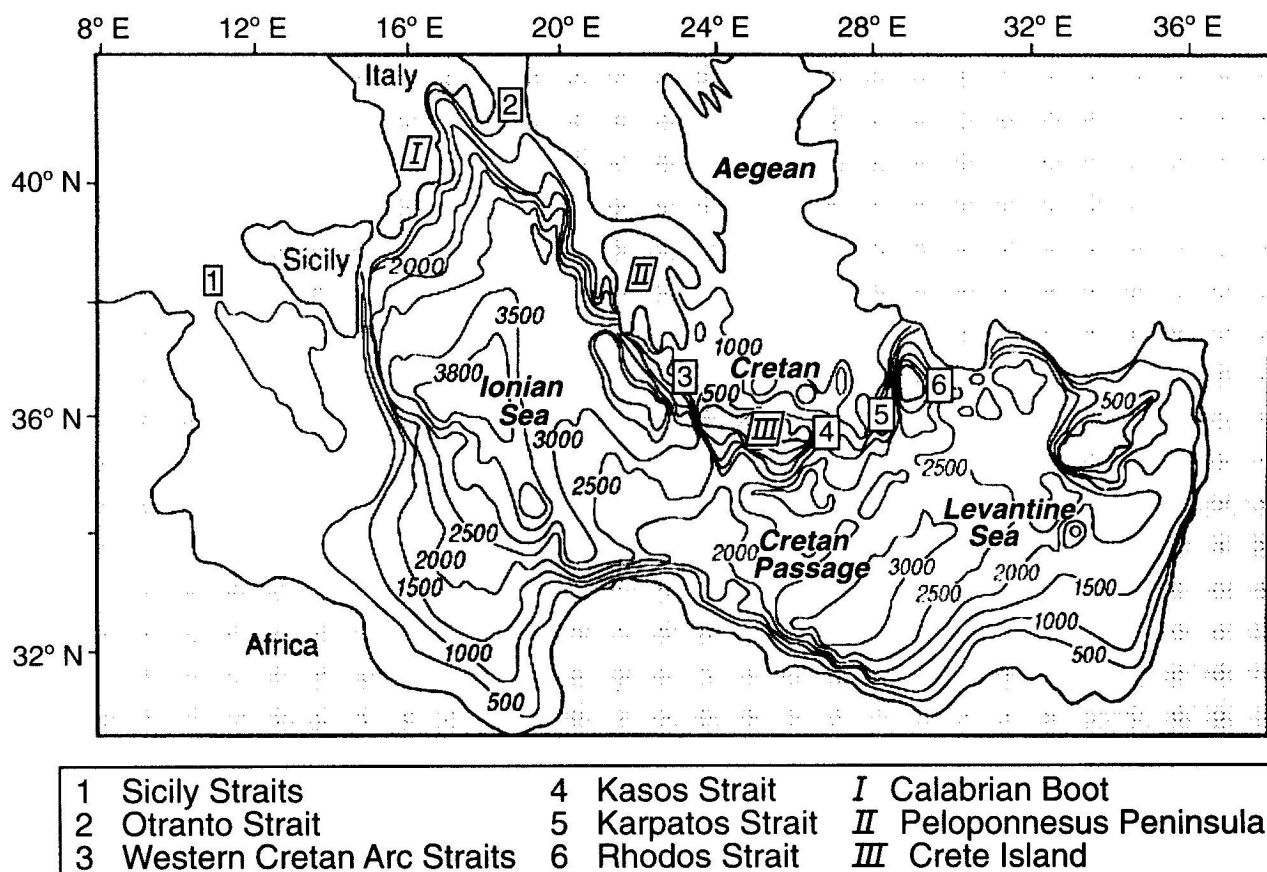
1. Introduction

[2] In the decade 1985–1995 the eastern Mediterranean has been the subject of very intensive research coordinated by the international collaborative program Physical Oceanography of the Eastern Mediterranean (POEM). The geometry and bathymetry of the basin are shown in Figure 1. The POEM program was the first to define the phenomenology of the major water masses and circulation features of the eastern Mediterranean [*United Nations Educational, Scientific, and Cultural Organization (UNESCO)*, 1984; *Malanotte-Rizzoli and Robinson*, 1988].

[3] Three dominant scales of motion are present. Two overall thermohaline cells exist, the first one connecting the eastern to the western Mediterranean, characterized by inflow of Atlantic Water (AW) at the Sicily Straits in the surface layer and by an outflowing, return flow of Levantine Intermediate Water (LIW) in the intermediate layer below (The water masses definitions follow the protocol established by CIESM Group, http://ciesm.org/events/RT5-WaterMassAeronyms.pdf.). This is the "open" circulation cell of the basin. The second thermohaline circulation is closed and confined to the eastern Mediterranean itself. It is driven by localized deep convection sites leading to the formation of the deep/bottom water masses that spread in the deepest layers, with subsequent upwelling and warm return flow in the intermediate layer. The second scale of motion is the subbasin, i.e., the upper thermocline circulation characterized by permanent or quasi-permanent gyres and cyclonic/anticyclonic structures connected by the intense jets and meandering currents. Finally, a mesoscale, ubiquitous and energetic, eddy field modulates the two larger scales all over the basin [*POEM Group*, 1992; *Robinson and Malanotte-Rizzoli*, 1993; *Malanotte-Rizzoli et al.*, 1997].

[4] In 1990, POEM evolved into POEM-BC (Biology and Chemistry), a fully interdisciplinary program with the

[1]P. Malanotte-Rizzoli, B. B. Manca, Salvatore Marullo, M. Ribera d' Alcala', W. Roether, A. Theocharis, A. Bergamasco, G. Budillon, E. Sansone, G. Civitarese, F. Conversano, I. Gertman, B. Herut, N. Kress, S. Kioroglou, H. Kontoyannis, K. Nittis, B. Klein, A. Lascaratos, M. A. Latif, E. Ozsoy, A. R. Robinson, R. Santoleri, D. Viezzoli, and V. Kovacevic.

| 1	Sicily Straits	4	Kasos Strait	I	Calabrian Boot
2	Otranto Strait	5	Karpatos Strait	II	Peloponnesus Peninsula
3	Western Cretan Arc Straits	6	Rhodos Strait	III	Crete Island

Figure 1. Configuration and bathymetry of the eastern Mediterranean. The names of the major subbasins and straits connecting them are given.

major objective of establishing the basin phenomenology for the chemical/biological components [*UNESCO*, 1992]. Interdisciplinary general surveys of the entire basin were carried out in 1991 and in 1992. In winter 1995 the field work culminated in a major observational effort, the Levantine Intermediate Water Experiment (LIWEX), aimed at mapping the history of the convective chimney of the Rhodes Gyre and the related water masses formation during its successive phases [*Malanotte-Rizzoli et al.*, 1996]. The LIWEX experiment was initiated with the second transient tracer survey of the basin carried out by the R/V *Meteor* (Germany), after the first one of POEM-V carried out in 1987, aimed at studying the preconditioning status of the eastern Mediterranean.

[5] This second tracer survey first showed the strong changes in the deep and bottom water masses of the eastern Mediterranean, the so-called Eastern Mediterranean Transient (EMT), i.e., the strong change in the closed thermohaline cell between 1987 and 1995. In 1987 the closed internal cell was driven by a deepwater formation source located in the southern Adriatic, leading to the spreading of Adriatic Deep Water (ADW) out of the Otranto Strait (Figure 1), becoming the Eastern Mediterranean Deep Water (EMDW) that reached the eastern Levantine. The renewal time of deep/bottom waters below 1200 m was evaluated to be of ~125 years [*Roether and Schlitzer*, 1991;

Schlitzer et al., 1991; *Roether et al.*, 1994, 1998, 1999; *Roether and Well*, 2001]. In 1995 the "engine" of the closed thermohaline circulation was instead the Aegean Sea leading to the formation of warmer, saltier and denser water masses, namely the Cretan Deep Water (CDW) [*Theocharis et al.*, 1999], that, exiting from the Cretan Arc Straits (Figure 1), spreads throughout the basin pushing to the west in the Ionian Sea and to the east in the Levantine the less dense EMDW of Adriatic origin [*Roether et al.*, 1996; *Klein et al.*, 1999, *Roether and Well*, 2001]. An in-depth analysis of the data collected during the 1991 October general survey of POEM-BC revealed that the EMT had actually started earlier, between 1987 and 1991 [*Malanotte-Rizzoli et al.*, 1999]. The evolution of the deep water masses in the source region of the Cretan Sea/southern Aegean Sea between 1986 and 1997 is analyzed in detail by *Theocharis et al.* [1999]. These studies showed that in 1991 the Cretan/Aegean Sea was already the driving "engine" of the intermediate to deep layer circulations, with Cretan Intermediate Water (CIW), Cretan Deep Water (CDW) and transitional Cretan water in-between spreading from the Cretan Sea (southern Aegean) into the basin interior.

[6] The study by *Malanotte-Rizzoli et al.* [1999] also revealed two major changes in the upper thermocline circulation and water mass pathways most probably connected with the EMT and possibly produced by the
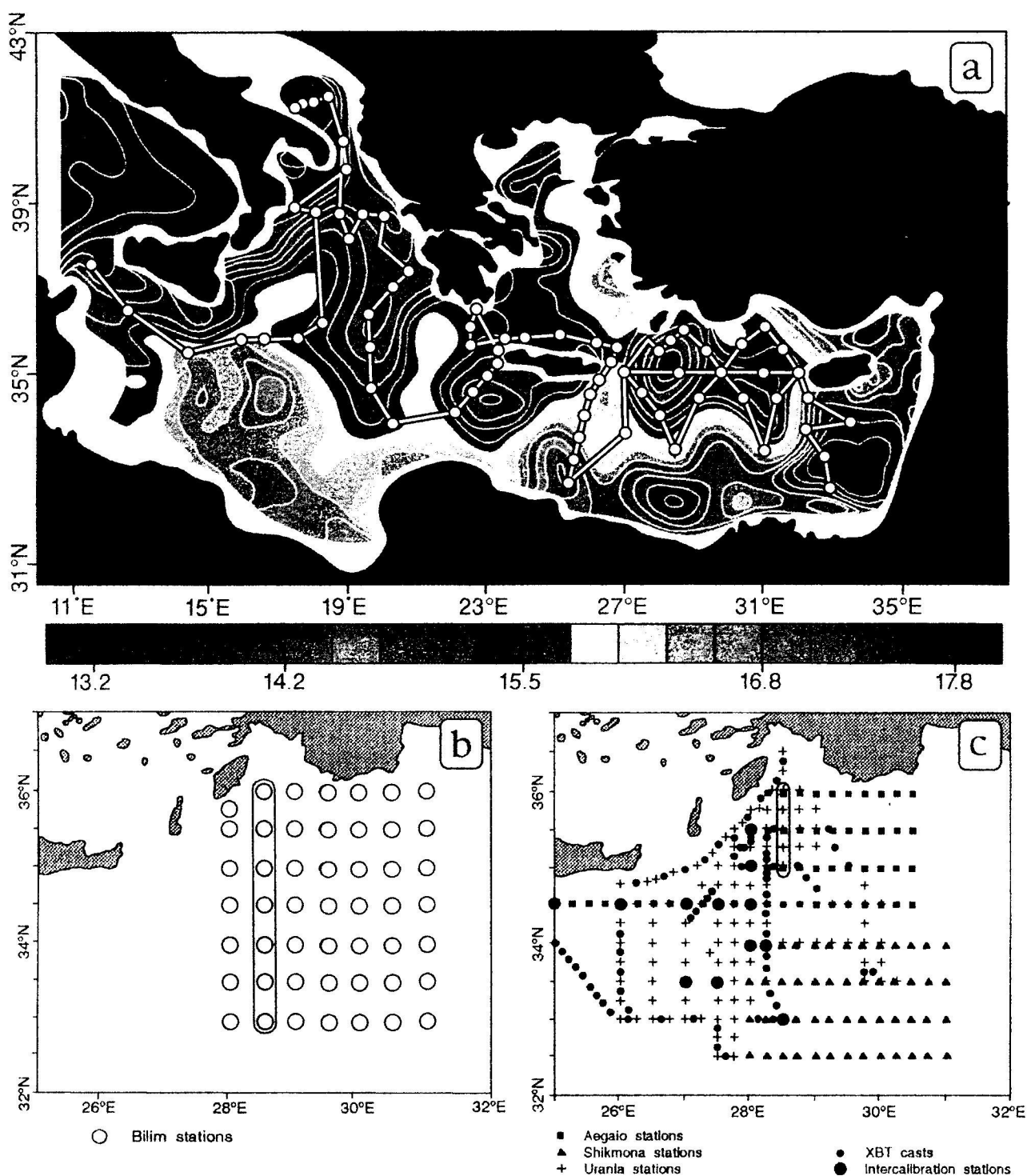
Figure 2. (a) Network of the January 1995 survey of the R/V *Meteor* (Germany) superimposed on a map of the temperature at 125 m depth. Large dots indicate hydrographic and tracer stations. (b) Network of the February 1995 survey of the R/V *Bilim* (Turkey). (c) Network of the survey of March–April 1995 carried out simultaneously by the R/Vs *Urania* (Italy), *Aegaio* (Greece), and *Shikmona* (Israel). The yellow section in Figures 2b and 2c is the one used for intercalibration. See color version of this figure at back of this issue.

important change in the wind stress field between the 1980s and the 1990s [*Samuel and Haines*, 1999; *Stratford and Haines*, 2002]. Specifically, the LIW formed in the Rhodes Gyre and, more generally, in the northern Levantine was blocked in its traditional westbound route to the Ionian Sea on its density horizons $\sigma_\theta = 29.05-29 \times 10$ kg m^{-3} by a three-lobe strong anticyclonic structure in the southern Levantine, that induced a substantial LIW local recirculation. LIW was replaced by more recent CIW in the Ionian Sea on the same density horizons. Furthermore, the strengthening of the anticyclonic circulation in the Ionian Sea caused the AW to recirculate massively in the Ionian interior with a consequent AW decrease in the Levantine sea. These changes persisted through 1995, as will be shown in the present investigation.

[7] The purpose of this study is to provide an in-depth analysis of the last POEM-BC field effort, namely the winter 1995 LIWEX experiment. The experiment was specifically planned to monitor the time evolution of the convective chimney of the Rhodes Gyre in the northern Levantine (Figure 2), which has been shown to be the location of winter time formation of LIW under the cold, dry north winds blowing from the continent [*Ovchinnikov and Plakhin*, 1984]. During exceptionally cold winters, the Rhodes Gyre has also been shown to be the formation site of Levantine Deep Water (LDW), fresher and colder than LIW, and hence denser [*Ozsoy et al.*, 1993; *Gertman et al.*, 1994].

[8] Dense water formation events in the Rhodes Gyre follows the "recipe" originally proposed by the *MEDOC Group* [1970] that consists of three phases. In the first one, the preconditioning phase, the progressive cooling occurring in the late fall season leads to a "doming" of the isopycnal surfaces in the formation region. The doming region is also characterized by a cyclonic circulation that upwells to the subsurface layer the cold deep waters. A further preconditioning process occurring in the Levantine Sea is due to the very intensive evaporation during the summer months that produces very salty water in the surface layer. The successive cooling in fall reduces so much the static stability of the water column that even minor wind events can induce vertical mixing throughout the intermediate layer.

[9] In the *MEDOC Group* [1970] recipe the preconditioning phase is followed by the "violent mixing" phase in which strong episodes of cold, dry winds from the mainland occur most frequently in January/February as evident from the wind stress climatology over the region [*May*, 1982]. Obviously, a strong interannual variability characterizes these events, leading to the formation of either LIW or LDW or of both. The latent heat loss can increase by more than one order of magnitude during these events and is accompanied by strong evaporation that increases the surface salinity. Both cooling and evaporation thus combine to increase the surface density to the point of breaking the weakened stratification. A strong convective cell is quickly established with full vertical mixing that can reach depths greater than 1000 m.

[10] At the end of the mixing phase, the third stage is constituted by the spreading and transformation phase, when the newly formed water mass(es) spread along isopycnal surfaces from the periphery of the convection site
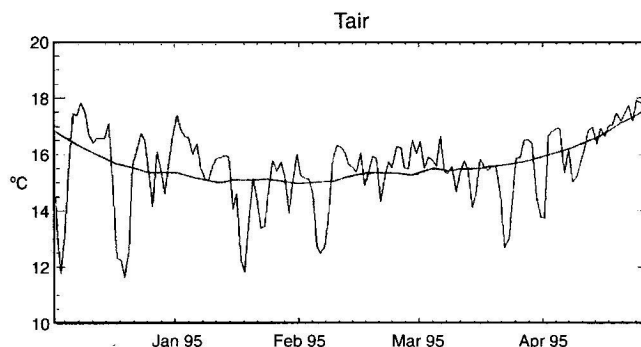
Figure 3. Low-frequency component of air temperature obtained by moving average with 50 weighting points. Time series of air temperature in °C from December 1994 to April 1995 At 35°N, 28.5°W near the center of the Rhodes Gyre. A running mean is superimposed.

toward the different parts of the basin, been veered in their pathways by the cyclonic/anticyclonic structures of the upper thermocline circulation.

[11] The LIWEX experiment of winter 1995 was designed to cover these successive phases and document the "history" of the convective chimney. In January 1995 the German R/V *Meteor* covered the Rhodes Gyre and western Cyprus cyclones, simultaneously carrying out the full basin transient tracer survey. The *Meteor* track is shown in Figure 2a, superimposed to the temperature distribution at 125 m depth.

[12] In February 1995 field work concentrated on the Rhodes Gyre itself, with the Turkish R/V *Bilim* covering the dense network of stations shown in Figure 2b. In late March/April a coordinated survey was carried out by the Greek R/V *Aegaio*, the Italian R/V *Urania* and the Israeli R/V *Shikmona* simultaneously at sea. The network of stations of this final survey is shown in Figure 2c. The nomenclature of the various cyclonic/anticyclonic structures used is the one presented by *Malanotte-Rizzoli et al.* [1999]. Focusing on the Rhodes Gyre chimney, the surveys did not cover the northern, eastern and southern periphery of the basin, where multiple sites of LIW formation may be present, as shown by the observational evidence of POEM-Phase I where LIW was found to be ubiquitous throughout the basin including the southern sector [*POEM Group*, 1992].

[13] The paper is organized as follows. In section 2 the time evolution of the atmospheric air-sea fluxes is presented to identify the cold outbreaks of strong winds possibly leading to deep convective mixing. In section 3 the circulation patterns and water masses are analyzed during the January survey. In section 4 the mid-February survey is analyzed. In Section 5, the analysis of the joint March/April survey is presented identifying the spreading pathways of the newly formed water masses. In section 6 we quantify the surface buoyancy flux and the related change of buoyancy content in the Rhodes Gyre throughout the experiment. Finally, in section 7, an overall discussion is given summarizing the major novel results of this work.

[14] In the following, the hydrographic properties are expressed as potential temperature (θ), salinity (S) according

Wind Speed squared ($u^2 + v^2$)
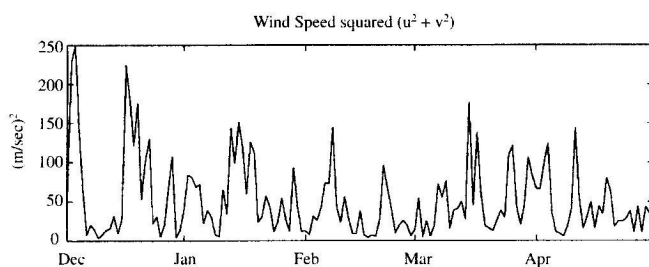
Figure 4. Time series of the wind speed (squared) for the same period of Figure 3 over the Rhodes Gyre.

to the practical salinity scale, density as potential density excess (σ_θ) and oxygen as dissolved oxygen in mL L^{-1}.

2. Time Evolution of Atmospheric Forcing During LIWEX

[15] In this section we investigate the time evolution of the SST and of the atmospheric forcing parameters in the Rhodes Gyre area, throughout the LIWEX period. The SST's are taken from NOAA AVHRR images and the ECMWF analysis of wind components (u and v), air temperature, relative humidity and cloud coverage is used to evaluate the various components of the heat budget through bulk formulas.

[16] In Figure 3 we present the time series of the daily average air temperature (T_{air}) from December 1994 to April 1995 at a geographical location near the centre of the Rhodes Gyre (35°N, 28.5°E; see Figure 2a). The low-frequency component of the air temperature (mean air temperature) was evaluated using a moving average over 50 consecutive data points. It decreases gradually from December to mid-January reaching a minimum average value of ~15°C which remains approximately constant through mid-February. Then the mean air temperature rises to 15.5°C through mid-March and finally from mid-March to the end of April a gradual increase occurs to ~18°C.
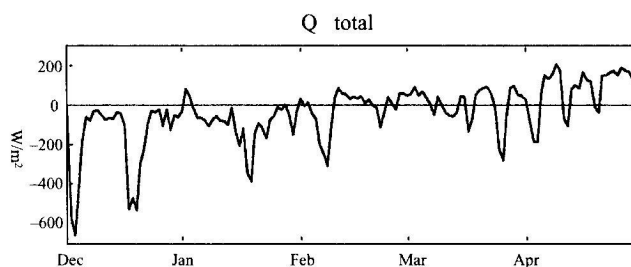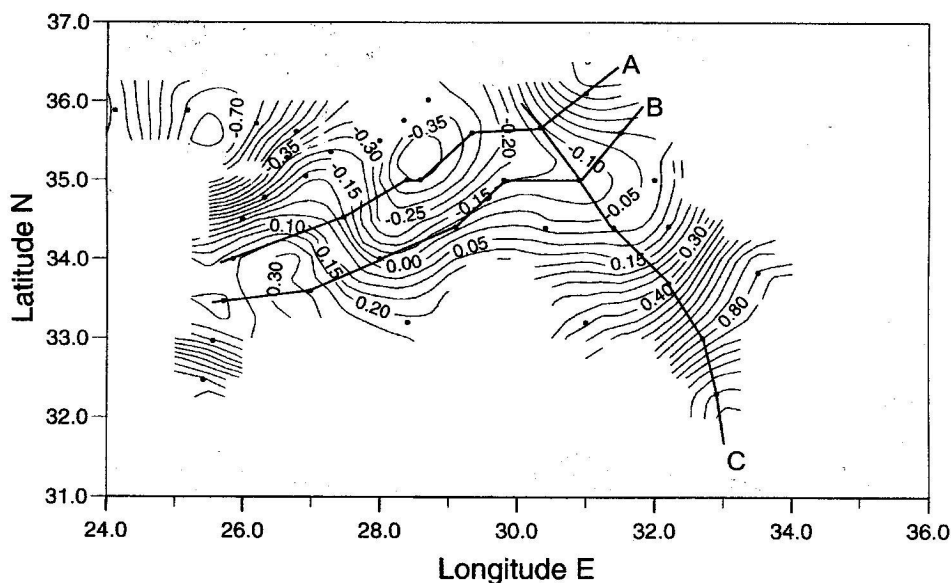
Q total

Figure 6. Time series of daily surface total heat flux in the same period of Figure 3 evaluated in the center of the Rhodes Gyre from bulk formulae.

Superimposed to this low-frequency variation are series of episodes in the synoptic timescale. The most important of such episodes occur in early and late December 1994, in mid-January and in early February 1995. As it can be seen from Figure 4, all four events are correlated with strong northerly wind outbreaks (storms) over the Rhodes Gyre area, cold and dry, hence very effective in cooling the sea surface, both through latent and sensible heat loss. The latent heat loss is accompanied by intense evaporation that increases the surface salinity. Both effects contribute to increase the surface density and induce convective mixing. The sea surface temperature (SST) in the center of the Rhodes Gyre is shown in Figure 5, with the mean evaluated through polynomial best fitting. It has a decreasing trend from 15.2°C at the beginning of December to 14.2°–14.3°C in early February with local minima of about 14°C at the end of December, end of January and mid February. From the second half of February the mean temperature gradually increases reaching 15°C at the end of the first week of April, with a successive substantial increase to 17.7°C by the end of the month.

[17] The air-sea heat budget can be expressed as the difference between the net shortwave solar radiation (incoming minus reflected) absorbed by the sea surface Q_s;
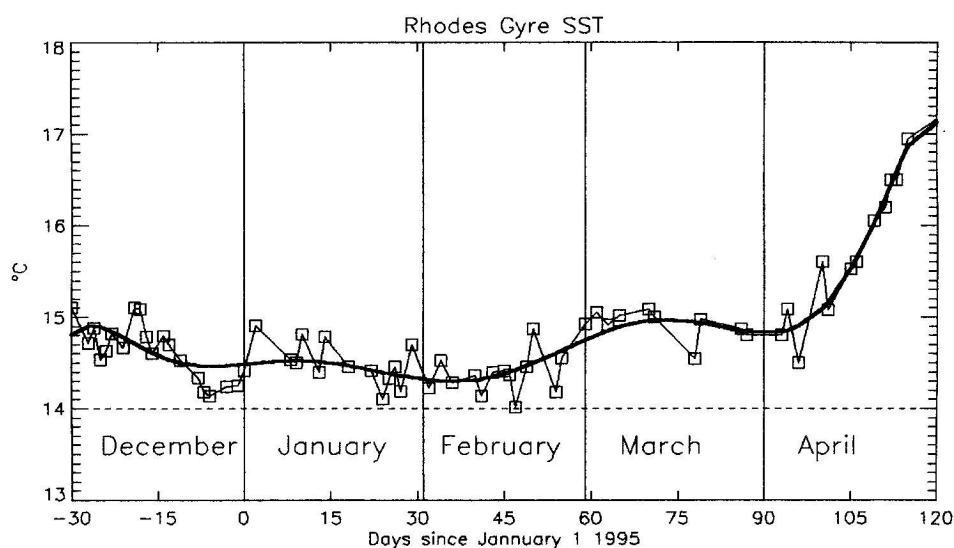
Rhodes Gyre SST

Figure 5. Time series of sea surface temperature (SST) in the center of the Rhodes Gyre inferred from AHVRR imagery.

Cruise R/V METEOR: Dyn. Height 0/800 dbar

Figure 7. Surface dynamic height anomaly with respect to 800 dbars during January 1995.

and the sum of the longwave back radiation Q_b, the sensible heat flux Q_h and the latent heat flux Q_e. Then the total heat flux (Q_t) is given by:

$$Q_t = Q_s - (Q_b + Q_h + Q_e).$$

[18] The calculation of the various components was carried out through appropriate bulk formulas that use the different atmospheric parameters (wind speed, air temperature, air humidity, and cloud cover) and the sea surface temperature [*Kondo*, 1975]. In our computations we have used the approach of *Castellari et al.* [1998] as the most appropriate for the Mediterranean. In Figure 6 we present the time series of daily surface total heat fluxes Q_t from December 1994 to April 1995 in the center of the Rhodes Gyre. We observe that from December to early February the center of the gyre shows a net heat loss to the atmosphere, then after a month of very small Q_t, there is an increasing net heat gain. These events are associated to frequent episodes of outbreaks of relatively dry and cold wind with drop of air temperatures as shown in Figures 3 and 4. The small but generally positive values of Q_t from mid-February to mid-March is related to the small increase of SST during the same period (Figure 5) which reduces both latent and sensible heat exchanges. The total heat flux evolution in the center of the Rhodes Gyre shows significant minima correlated to intense heat losses at timescales of the order of few days in early and mid-December of about -600 W m^{-2} and -500 W m^{-2}, respectively; while the heat losses were -400 W m^{-2} in mid-January and -300 W m^{-2} in early February.

[19] A major point emerges from the above results, that is winter cooling in 1995 seems to have started as early as the beginning of December. The most severe storms and cooling episodes occurred in fact during that month, while in January and February the episodes are less intense. As a

consequence the heat loss period in the gyre is shifted earlier by almost an entire month compared to the climatological winter, in which the severe storm events, and the related strong heat losses, are concentrated in February and early March. Both the beginning of the early winter and the late March transition to spring are clearly reflected in the SST's of Figure 5. In fact, in December the minimum temperature in the center of the Rhodes Gyre reached values as low as $14.1°-14.2°C$, a value usually encountered at the end of the climatological winter in February [*Lascaratos et al.*, 1993]. This early winter can be interpreted as being responsible for deepwater formation in the center of the gyre instead of the intermediate one because of the longer duration that the convective cell was ventilating to the atmosphere experiencing net heat loss. As shown in section 3a, by January 1995, at the time of the first survey, the convective cell was ventilating to the atmosphere and the mixing phase was already ongoing. Hence the preconditioning phase most probably occurred in late 1994, probably as early as November.

3. Circulation Pattern During January Phase of LIWEX

[20] The surface dynamic height anomaly with respect to 800 dbar (Figure 7), analyzed from the January 95 *Meteor* survey shows the upper thermocline main circulation features in the Levantine. Because of the rather coarse resolution of the survey network (stations marked with dots in Figure 7), a fine structure mapping of the circulation cannot be made. The overall major features can nevertheless be unambiguously identified. The cyclonic Rhodes Gyre southeast of Rhodes covers a broad area extending roughly from 28° to 30°E and from 34.5° to 36°N. The western Cyprus cyclone, observed further to the east and in the same location during the previous POEM surveys [*POEM Group*,
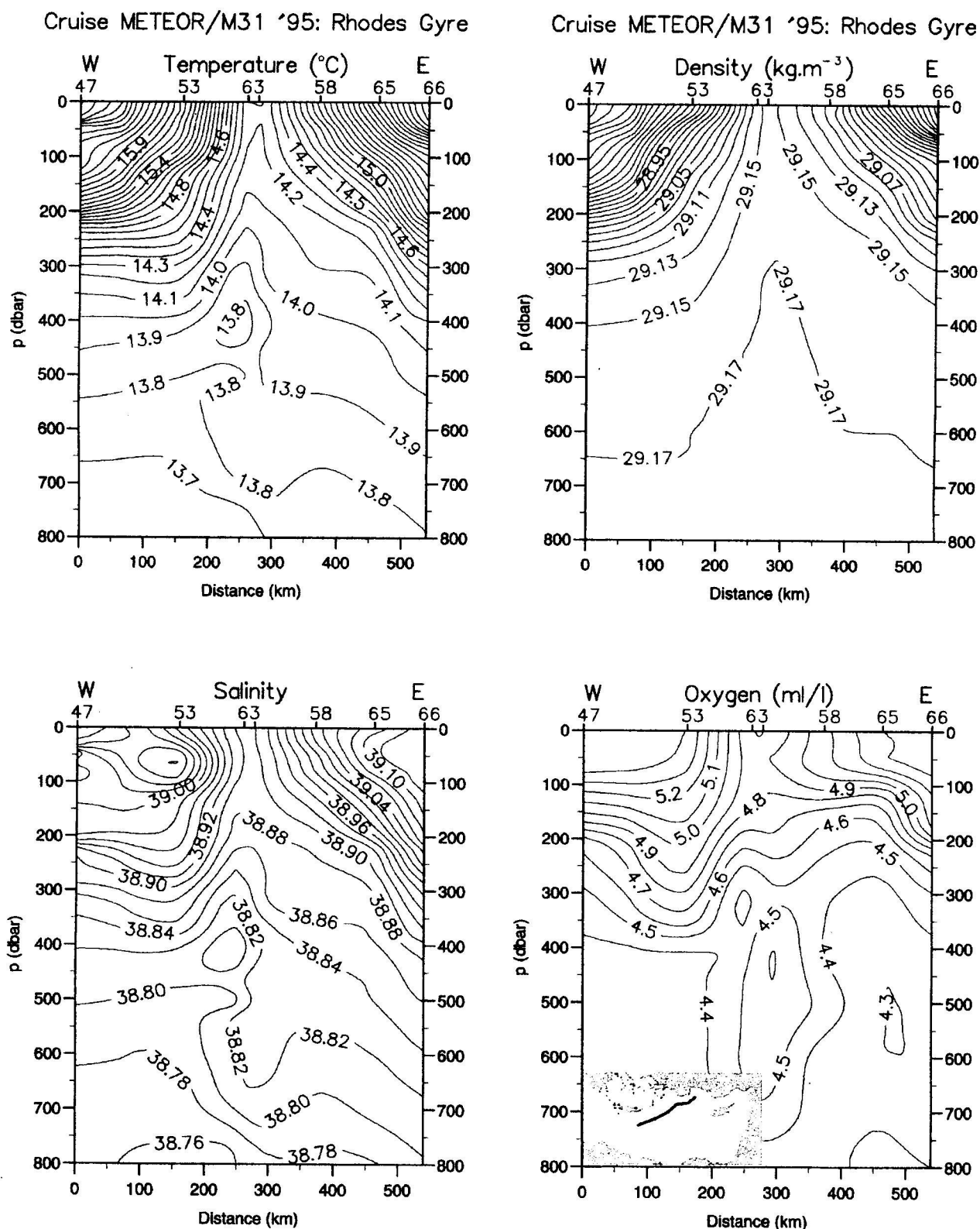
Figure 8.   The ventilated chimney of the Rhodes Gyre in January 1995 along section A of Figure 7, also marked in the inset.

1992], is connected to the Rhodes Gyre by the Central Levantine Basin Current [*Ozsoy et al.*, 1993], which broadly encloses the overall cyclonic region in the northern Levantine. This cyclonic circulation extends longitudinally from the Eastern Cretan Arc Straits to Cyprus and is bounded in the north by the Asia Minor Current (AMC) which flows westward along the Turkish coastline. To the southwest of the Rhodes Gyre the Ierapetra anticyclone is barely captured
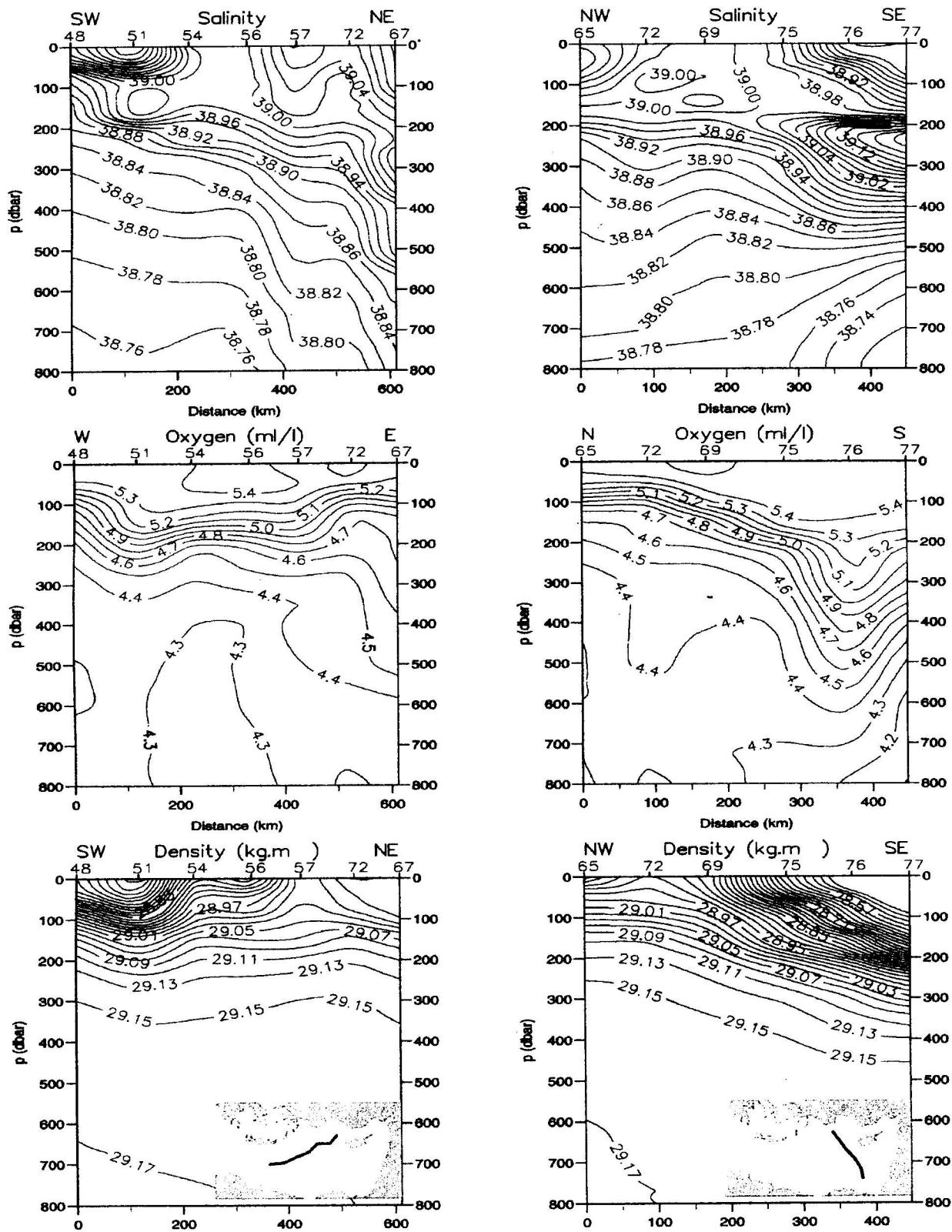
Figure 9. Distributions of salinity, oxygen, and potential density in January 1995 along (left) section B and (right) section C of Figure 7. The sections are shown in the insets.
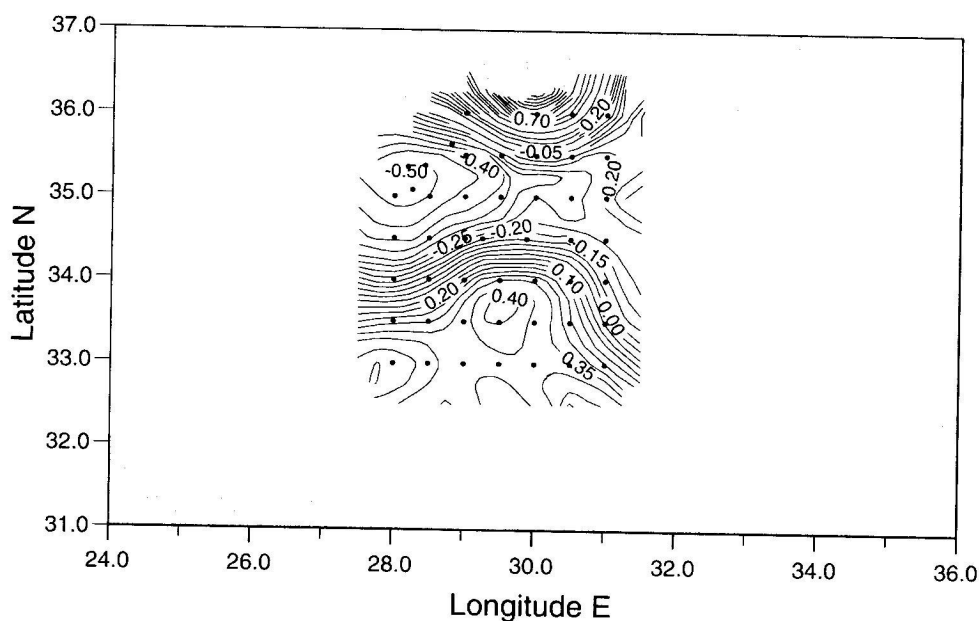
Cruise R/V BILIM: Dyn. Height 0/800 dbar

Figure 10. Surface dynamic height anomaly with respect to 800 dbars in February 1995.

in Figure 7. Three sections marked A, B, and C in Figure 7 will be analyzed in the following.

3.1. Ventilated Chimney Inside the Rhodes GYRE

[21] Temperature, salinity, density and oxygen vertical distributions in the upper 800 m are shown in Figure 8 along section A shown in the insert that crosses the center of the Rhodes Gyre. They clearly show that the chimney was indeed ventilating during January 1995, with isotherms, isohalines and isopycnals outcropping to the surface and defining the chimney core. In the temperature pattern the first outcropping isotherm has $\theta = 14.3°C$ and the chimney core is weakly stratified with isotherms doming to ~400 m depth. The salinity distribution of Figure 8 shows that the chimney core is marked by a surface salinity minimum S = 38.90 reaching the value of 38.96–38.98 at its periphery. The chimney is also weakly stratified in the salinity patterns, with doming of isohalines down to ~350 m. As evident from the core values of (θ, S), in winter 1995 LDW was formed inside the Rhodes Gyre rather than LIW. Typical ranges for LDW are in fact $\theta \simeq 13.7°–14.5°C$ and S $\simeq$ 38.8–38.9 [Ozsoy et al., 1993; Gertman et al., 1994] ,while the LIW signature is marked by S $\geq$ 39.00 and $\theta > 15°C$. In Figure 8 the fresher core of the chimney is enclosed between two tongues of saltier water, the first one protruding from the southwest (S = 39.02); the second one, much saltier (maximum S = 39.10) protruding from the northeast.

[22] The weak temperature and salinity stratifications of Figure 8 compensate in the density distribution that shows a well-defined ventilating chimney with the first outcropping isopycnal at $\sigma_\theta = 29.15$ kg m^{-3} and a core reaching a maximum density of 29.17 kg m^{-3} at ~600 m depth. Again, such high-density values are typical of LDW.

[23] The oxygen distribution of Figure 8 shows an oxygen surface value of 4.9 mL L^{-1} in the ventilating

region. A core with a secondary oxygen maximum is present in the intermediate layer. This secondary maximum of 4.5 mL L^{-1} found at ~500 m depth in the chimney may be the signature of an older water mass formed during a previous convective event as it will be discussed in section 4.

3.2. LIW Formation in the Northern Levantine

[24] If LDW has formed inside the Rhodes Gyre, proper LIW was instead formed in the northeastern Levantine, along the Turkey coastline. Figure 9 shows two sections crossing the basin diagonally, section B (left panels) and section C (right panels) of Figure 7. The section tracks are also shown in the inset maps.

[25] The property distributions along section B, left panels of Figure 9, show the presence of a shallow ventilating chimney in the northeastern extremity, with the outcropping isopycnal $\sigma_\theta = 29.01$ kg m^{-3} delimiting the chimney core. Doming of isopycnals is evident only to ~100 m depth, corresponding to densities of 29.03– 29.05 kg m^{-3}. The chimney is centered near station #57 and is characterized by a surface salinity maximum of 39.06 and an oxygen maximum of 5.3–5.4 mL L^{-1}, the latter indicating ventilation to the atmosphere. The salinity and density values as well as the shallowness of the thermostad characterize the chimney water mass as typical LIW.

[26] A second ventilating chimney, even shallower, is present in section C, right panels of Figure 9, near station 72 in the northwestern extremity of the section. The core properties are here lighter, but still in the LIW range, with $\sigma_\theta = 28.95–29.00$ kg m^{-3}, salinity ~39.00 and again high-oxygen values, 5.4 mL L^{-1}. Both chimneys appear to be events occurring inside the overall cyclonic circulation of the northern Levantine.

[27] The LIW formation process in these shallow chimneys does not follow the recipe leading to deep
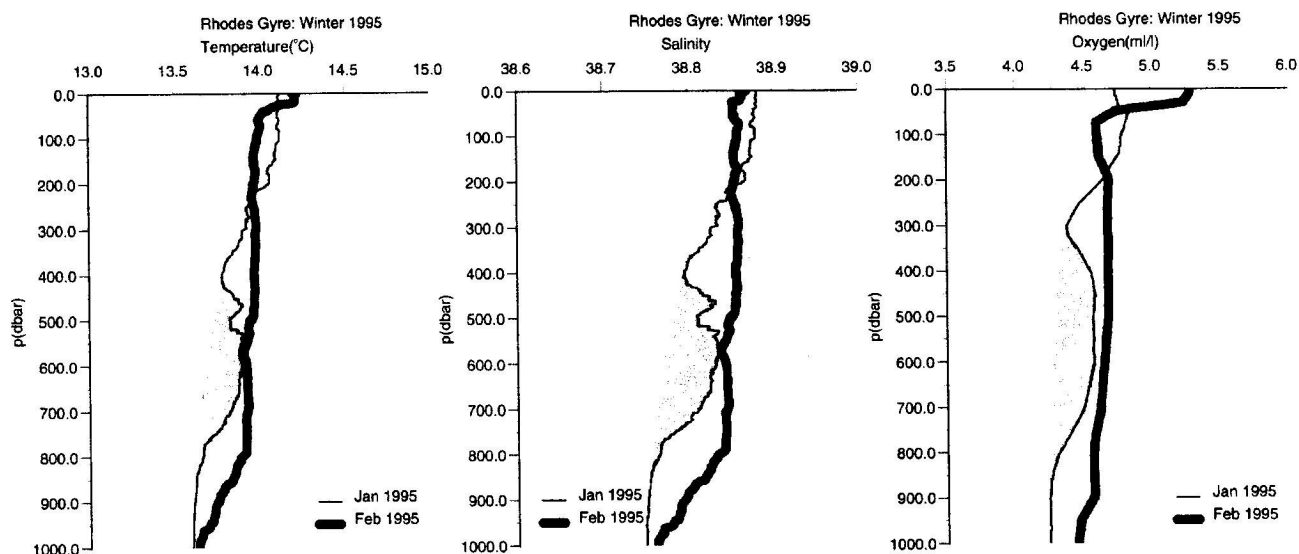
Figure 11. Comparison of the averaged vertical profiles of temperature, salinity, and oxygen in January (thin line) and February (thick line) at stations inside the Rhodes Gyre chimney.

convection and deepwater mass formation. Even in the absence of severe storm events, winter surface cooling and evaporation are sufficient to produce in coastal regions shallow, well mixed thermostads of LIW similar to the thermostads of Mode Waters formed throughout the world ocean [McCartney, 1982]. When the newly formed LIW subducts migrating away from the ventilating region, it spreads on the isopycnal surface delimiting its basis to conserve its potential vorticity. In both chimneys the high-salinity water mass (S greater than 38.98) appears to be sliding sideways along the isopycnal surfaces (left) 29.01–29.05 and (right) 28.95–28.98.

4. Circulation Patterns During the February Phase of LIWEX

[28] The last major outbreak of cold, dry winds from the mainland occurred around 10 February (Figure 6), with the net heat loss Q_t reaching a maximum of ~-300 W m^{-2}. The intensive field survey of the Turkish R/V Bilim, shown in Figure 2b, was carried out during 10–17 February 1995. The circulation pattern is shown in the dynamic height anomaly map of Figure 10 of the surface relative to the 800 dbar level. The Rhodes Gyre extends from about 28° to 30°E, with its westernmost part not covered by the survey. The Rhodes Gyre is barely separated by the western Cyprus cyclone appearing at 31°E. Similarly to the January pattern of Figure 7, the entire northern half of the basin is comprised in an overall cyclonic circulation. In the north the westward flowing Asia Minor Current is observed along the Turkish coast. In the south, a strong, jet-like current, namely the Central Levantine Basin Current (CLBC) crosses the entire domain from west to east.
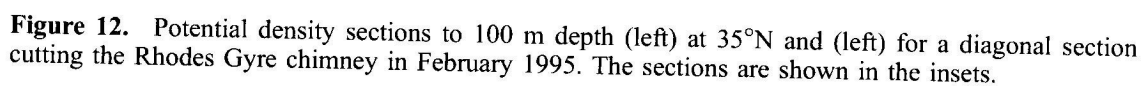
[29] The patch of relatively homogeneous water mass observed in January (Figure 8) became deeper and fully mixed in the 15-day interval before the February survey. The actual well-mixed chimney occupies now the region

35°–35°20'N, 28°–28°30'E and was surveyed on 15 February. At the 500 dbar level (not shown) the cyclonic circulation around the chimney persists in the northwestern corner of the domain of Figure 10. The comparison of the averaged vertical profiles at Bilim (February) and Meteor (January) stations inside the chimney core is shown in Figure 11.
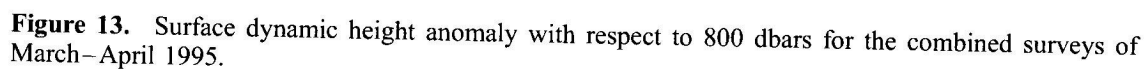
[30] In January the profiles of temperature, salinity and oxygen (thin lines) show a vertical homogenization limited to the upper 200 m. The chimney core reached $\sim$350 m depth with θ in the range 14°–14.1°C and S in the range of 38.86–38.88. A minimum in these two properties is reached at $\sim$400 m and at $\sim$300 m for oxygen. Between 400 and 800 m a layer of positive anomalies in θ, S, O$_2$ is found with respect to the corresponding deep values (shaded regions in Figure 11), with anomaly magnitudes of $\Delta\theta \sim 0.3$°C; $\Delta S \sim$ 0.1; $\Delta O_2 \sim 0.5$ mL L^{-1}. These significant anomalies are consistent with the signature of a dense water mass formed during an earlier convective event which persists at depth and is isolated from the most recently ventilated surface layer. The signature of this water mass is lost in February because of the stronger mixing event following the February cold outbreak.

[31] On 15 February, after the cooling event of 10 February, the water column is vertically homogeneous. Potential temperature is constant at $\sim$13.96°C down to 800 dbar apart from the top 50 dbar where stratification begins to be reestablished after the cold outbreak (Figure 11). Salinity, on the other hand, is constant at S = 38.86 from the surface to 800 dbar. The θ/S values and the depth of the well-mixed chimney show that in winter 1995 the Rhodes Gyre was the formation site of LDW, colder and fresher than LIW, and rather denser ($\sigma_\theta = 29.18$ kg m^{-3}). The profile of dissolved oxygen, measured by the Winkler analyses of discrete samples, shows a fairly homogeneous distribution down to 1000 m depth.

[32] Figure 12 shows the potential density zonal section at 35°N (left panel) and a diagonal section across the chimney

Figure 12.   Potential density sections to 100 m depth (left) at 35°N and (left) for a diagonal section cutting the Rhodes Gyre chimney in February 1995. The sections are shown in the insets.

(right panel). In the zonal section the well-mixed chimney is localized in the westernmost part, between 28° and 28.5°E (left panel), with the homogeneous water mass at $\sigma_\theta >$ 29.17 kg m^{-3} extending down to 1000 dbar. In the diagonal section (right panel) the well-mixed chimney is even more evident with the typical doming of isopycnals 29.16–29.17 kg m^{-3} and a well mixed core with $\sigma_\theta >$ 29.17 kg m^{-3}. Figure 12 confirms the beginning of recapping in the

Figure 13.   Surface dynamic height anomaly with respect to 800 dbars for the combined surveys of March–April 1995.

LIWEX95: Section lerapetra–Rhodes Gyre

Temperature (°C)

LIWEX95: Section lerapetra–Rhodes Gyre

Density (kg.m⁻³)

Salinity

Oxygen (ml/l)
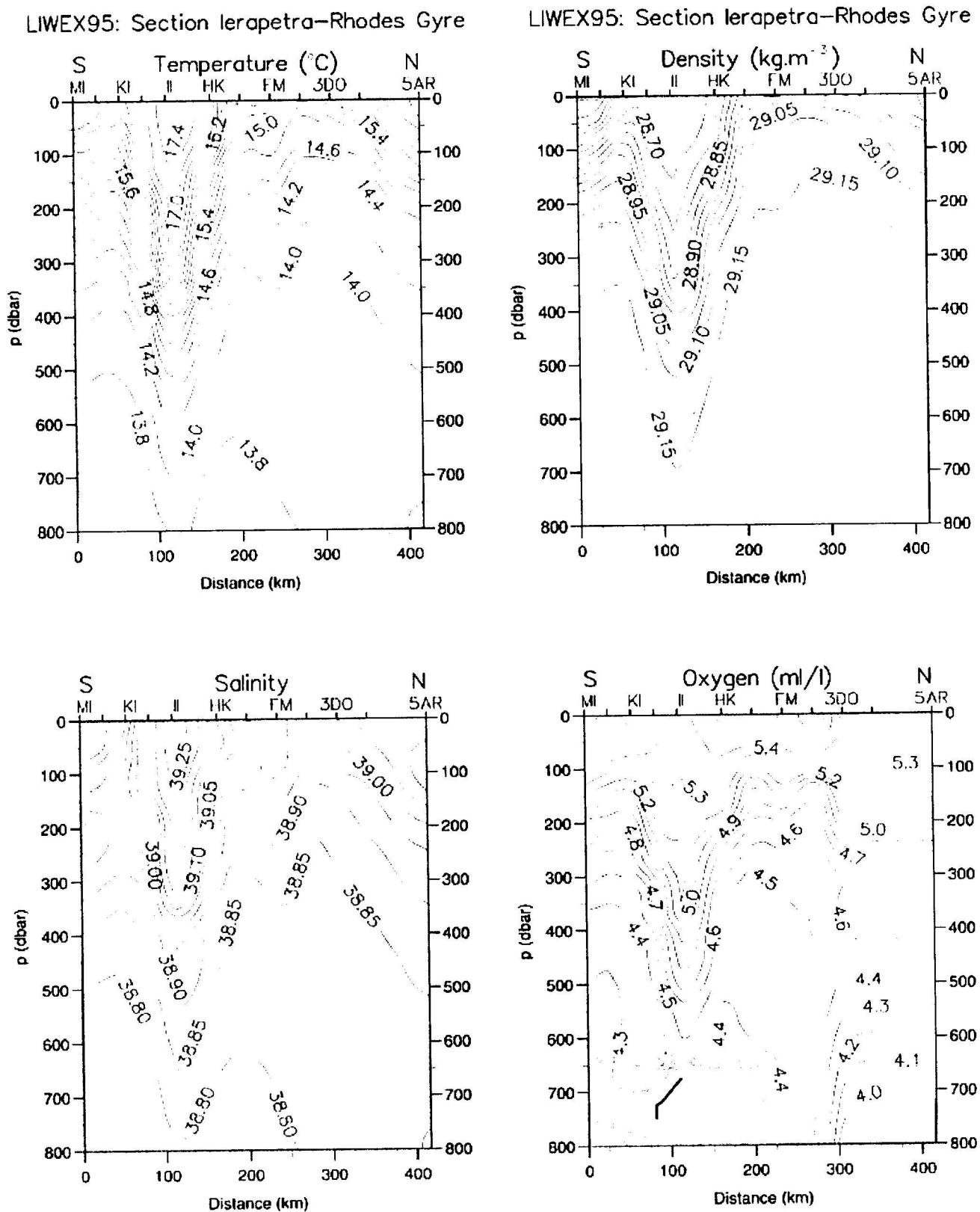
Figure 14. Vertical distribution of properties to 800 m depth along a section crossing the Ierapetra anticyclone and the Rhodes Gyre during March–April 1995. The section is shown in the inset.
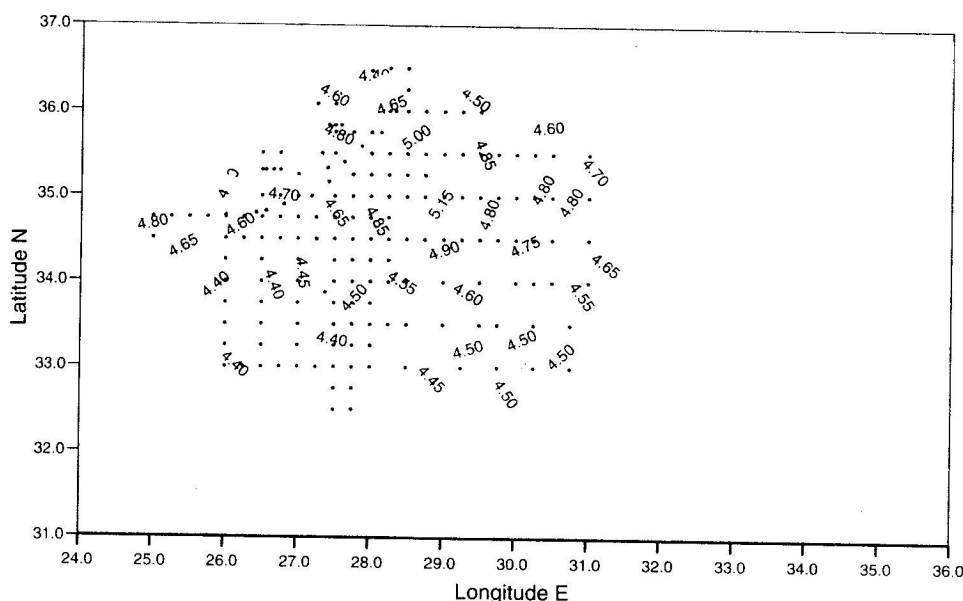
Cruise LIWEX '95: Oxygen at density=29.15 kg/m3

Figure 15. Oxygen pattern on the LDW isopycnal surface 29.15 Kg m^{-3} during March–April 1995.

top 50 dbar observed in Figure 11 because of the surface warming that followed the cold outbreak of 10 February.

5. Circulation Patterns During the March–April Phase of LIWEX: The Spreading Phase

[33] The March–April survey (Figure 2c) was designed to detect the pathways of newly formed waters from the formation site to the neighboring regions. The station grid spacing was 1/4° in zonal and 1/2° in meridional direction, with the boundaries at 26°E and 31°E . The station grid was also denser along the Eastern Cretan Arc Straits to monitor the exchanges between the Levantine and Aegean basins [Manca et al., 1999].

[34] The subbasin-scale upper thermocline circulation is captured by the dynamic height anomaly map of the surface with respect to the 800 dbar level, shown in Figure 13. In the north, a broad cyclonic Rhodes Gyre with its northern boundary constituted by the Asia Minor Current flowing westward along the Turkish coast and entering into the Aegean Sea through the Karpathos Strait. A strong, jet-like current separates the northern cyclonic area from a southern anticyclonic region. At the entrance of the Levantine basin in the Cretan Passage, the MMJ bifurcates into two branches (Figure 13). The northern branch is the CLBC already observed in February (Figure 10) that flows eastward between the southern rim of the Rhodes Gyre and the northern rim of the Ierapetra and easternmost anticyclones. The southern branch, i.e. the actual MMJ in the Levantine basin, forms the northern boundary of the southern Mersa-Matruh anticyclone only partially covered by the survey.

[35] This large anticyclonic region is similar to the one observed in the 1991 October POEM-BC general survey [Malanotte-Rizzoli et al., 1999], that completely blocked the LIW pathway to the west into the Cretan Passage. The anticyclonic region of winter 1995 is also constituted by three lobes: (1) the westernmost one, at 34°N, 27°E is the

Ierapetra anticyclone; (2) the northern rim of the southern Mersa-Matruh anticyclone is captured by the survey between 32° to 33°N, and 26° to 29°E; (3) the third anticyclone, analogous to the one present in 1991, is centered at 33.5°N, 29.7°E.

5.1. Water Mass Pathways: LDW

[36] By the time of the March–April survey, the Rhodes Gyre shows considerable recapping as stratification is gradually restored by surface warming. Figure 14 shows the vertical distribution of properties along the section given in the inset crossing meridionally the Ierapetra anticyclone and then the Rhodes Gyre. The first feature to be noticed is the warm ($\theta \geq 16°C$), salty (S $\geq$ 39.05) and light ($\sigma_\theta \leq$ 28.95 kg m^{-3}) Ierapetra thermostad in the south confined to the upper 300 m. Maximum oxygen values, showing surface ventilation, are found in the core, $O_2 \geq 5.2$ mL L^{-1}. Notice that the Ierapetra anticyclone is filled by a water mass lighter than LIW, and hence rather shallower than the 29.00 LIW horizon in the same location (not shown).The isolines of θ, S, σ_θ connected to the northern Rhodes Gyre are pushed downward by the Ierapetra thermostad.

[37] The northern Rhodes Gyre of Figure 14 can be compared with the January pattern of Figure 8 and the February one of Figure 12. In January the gyre was ventilating to the atmosphere (Figure 8). Recapping had already started by February, after the strong mixing event leading to LDW formation, but was limited to the surface 50 m (Figure 12). The LDW thermostad in April is confined between 200 and 800 m depth, characterized by the core values of $\theta = 14°C$; S $\cong$ 38.85, $O_2 \simeq 4.5$ mL L^{-1}and $\sigma_\theta =$ 29.15 kg m^{-3}. To follow the LDW fate, in Figure 15 the oxygen distribution is shown on the LDW horizon, $\sigma_\theta =$ 29.15 kg m^{-3}. No significant spreading is observed. The most oxygenated and salty water, the proper LDW, remains confined inside the Rhodes Gyre cyclonic circulation, not affecting the circulation of the Levantine basin outside its
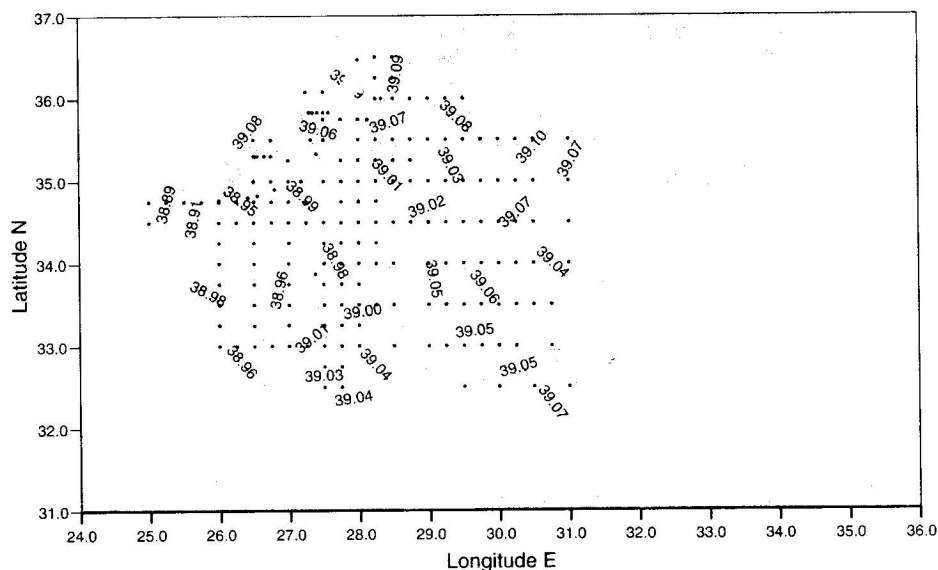
Cruise LIWEX '95: Salinity at density 29.00 kg/m3

Figure 16.   Salinity pattern on the LIW isopycnal surface 29.00 Kg m^{-3} during March–April 1995.

localized formation region. Topographic effects may be responsible for this trapping.

5.2.   Water Mass Pathways: LIW

[38]   LIW on the other hand appears to spread significantly from its northeastern formation sites. Figure 16 shows the salinity pattern on the isopycnal $\sigma_\theta = 29.00$ kg m^{-3}. The high resolution of the station grid of the March–April survey permits a good identification of the LIW pathways. The LIW pool is evident in the northeastern region near the Turkish coast, where the shallow ventilating chimneys were found in January (Figure 9), with maximum values $S \geq 39.10$. Two major LIW pathways seem to be present.

[39]   In the first pathway, LIW waters are entrained westward by the Asia Minor current. A bifurcation in the spreading occurs in front of the East Cretan Arc, with a first branch of salty isohalines entering into the Aegean south of Rhodes. This intrusion of LIW into the Aegean and Cretan seas may have been an important factor in preconditioning the southern Aegean surface waters, leading to increasing volumes of CIW and CDW under severe winter conditions, as shown in the modeling study by *Samuel and Haines* [1999]. After the bifurcation, the second branch of LIW flows cyclonically around the Rhodes Gyre, with successive entrainment in the CLBC indicated by the eastward protruding salty tongue at 33.5°N, where the CLBC forms a strong mender (Figure 13).

[40]   In the second pathway of Figure 16, the LIW protrudes directly southward from the northern formation region and reaches the eastern anticyclone at 33.5°N, 29.7°E. The pattern shown in Figure 16 suggests the possibility of LIW directly sliding into this eastern anticyclone.

[41]   To confirm the above interpretation of LIW pathways, property distributions have been mapped on vertical sections cutting the basin both meridionally and zonally. The first pathway, cyclonic around the Rhodes Gyre, is captured in a section that cuts the basin meridionally at

28°E and is shown in Figure 17 with the distributions of temperature, salinity, oxygen and density. The section cuts the LIW entrained westward by the Asia Minor Current in the northern end, marked by an arrow; and the LIW entrained eastward by CLBC in the southern end, also marked by an arrow (Figure 16). The layer with $S \geq 38.95$, shaded in gray, is centered around the LIW horizon of $\sigma_\theta = 29.00$ Kg m^{-3} ,indicating that LIW is also present in the basin interior, between the two oppositely flowing northern and southern veins. The same isopycnal is marked in the oxygen distribution showing the high-oxygen content of the LIW waters.

[42]   The second pathway pf LIW protruding southward from the northern formation region (Figure 16) is captured by the zonal section at 34°N shown in Figure 18. A vein of LIW with $S \geq 39.00$ and high-oxygen content $O_2 \geq 5$ mL L^{-1}, shaded in gray, is found at ~200 m on the eastern side, between 29° and 30°E, at the southern end of the salty tongue of Figure 16. Again, the vein is centered around the LIW horizon 29.00 Kg m^{-3}. The fate of this second vein is again eastward entrainment by the CLBC (Figure 13).

6.   Surface Buoyancy Flux and Buoyancy Content Change in the Rhodes Gyre Area

[43]   The process responsible for dense water formation is the buoyancy loss of the surface water mass due to surface cooling during winter storms. In section 2 the time series was shown of daily surface net heat flux in winter 1995. Here we focus on the time evolution of the surface buoyancy flux to explain to what extent the atmospheric forcing may account for the buoyancy content change and dense water formation process. The time series of the surface buoyancy flux over a longer time period, from October 1994 to April 1995, and the observed hydrographic structure in the Rhodes Gyre are analyzed to evaluate the correlation between the variability of the buoyancy fluxes and the buoyancy content changes.
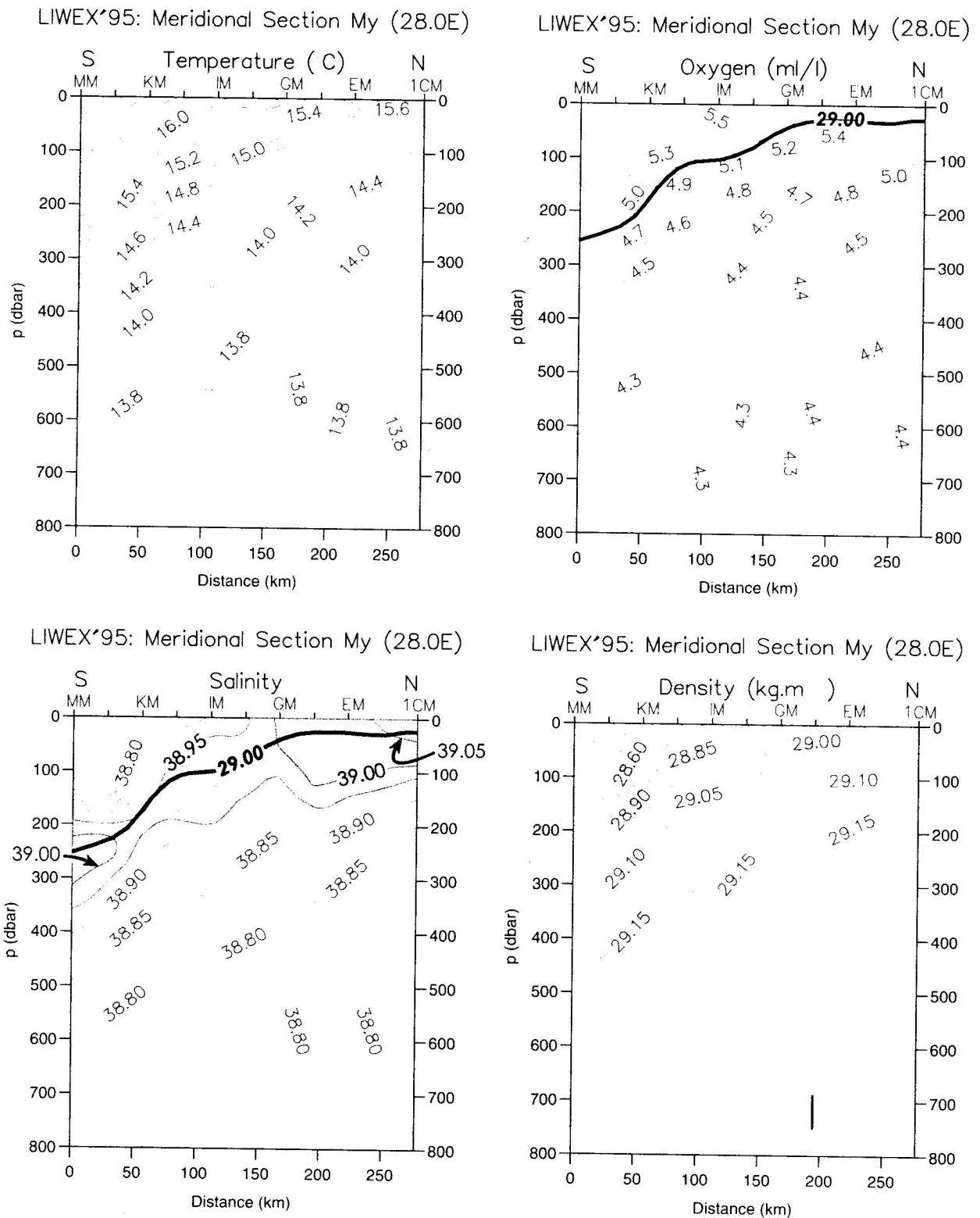
Figure 17. Property distributions along a meridional section at 28°E. The section is shown in the inset. The isopycnal surface 29.00, marked in the figures, is centered in the LIW layer, shaded in gray.
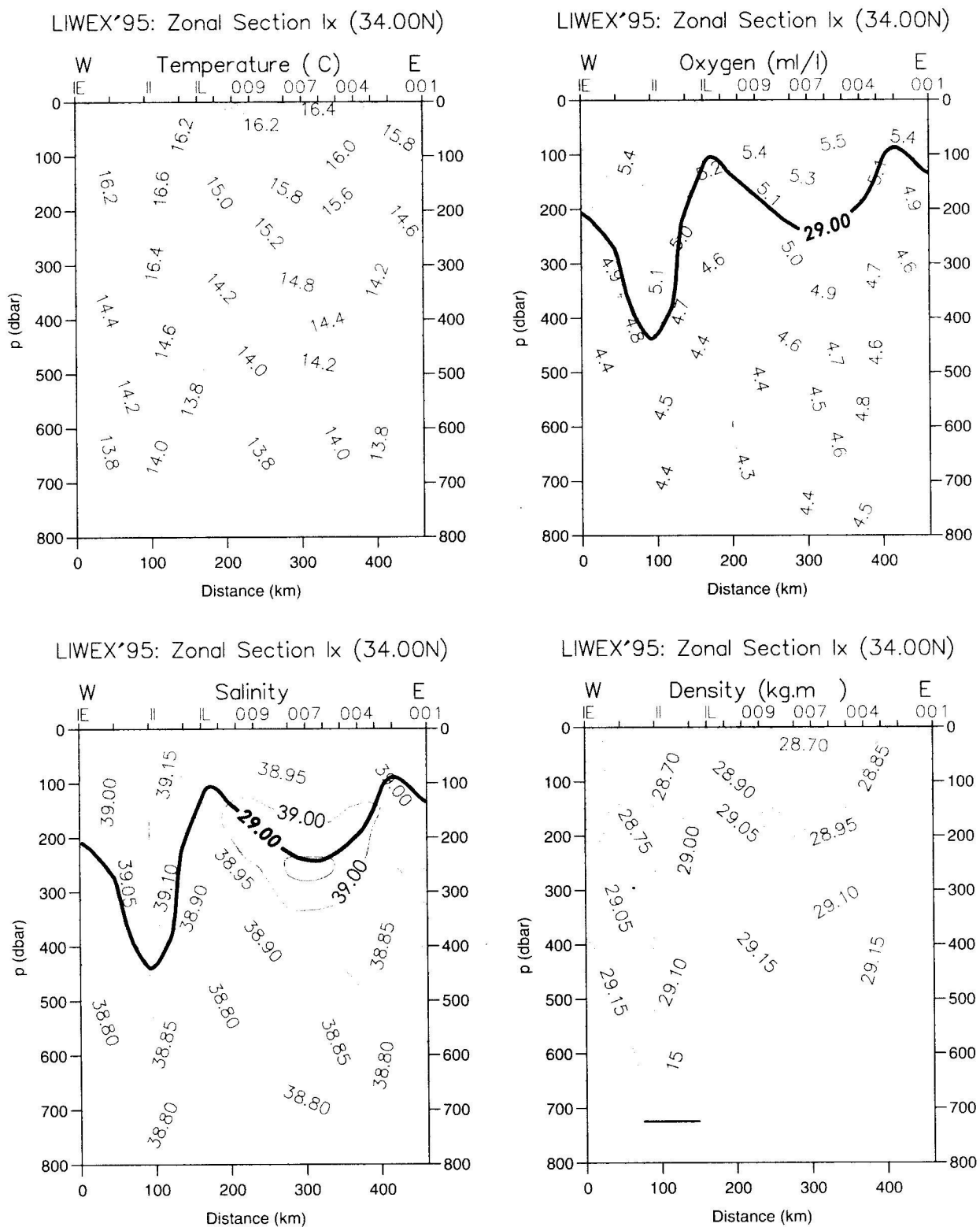
Figure 18. Property distributions along a zonal section at 34°N. The section is shown in the inset. The isopycnal surface 29.00, marked in the figure, cuts a tongue of LIW spreading southward in the eastern side, shaded in gray.

[44] The details of the evaluation of the surface buoyancy flux B_0 (m^2 s^{-3}) and of the total buoyancy content are given in the Appendix A. Here we discuss only the results of the calculations. From the evolution of the surface buoyancy flux B_0 in the period 1 October 1994 to 30 April 1995, we evaluated the time series of the integrated buoyancy flux (not shown), which exhibited decreasing negative values (buoyancy loss) from the first week of November until mid-
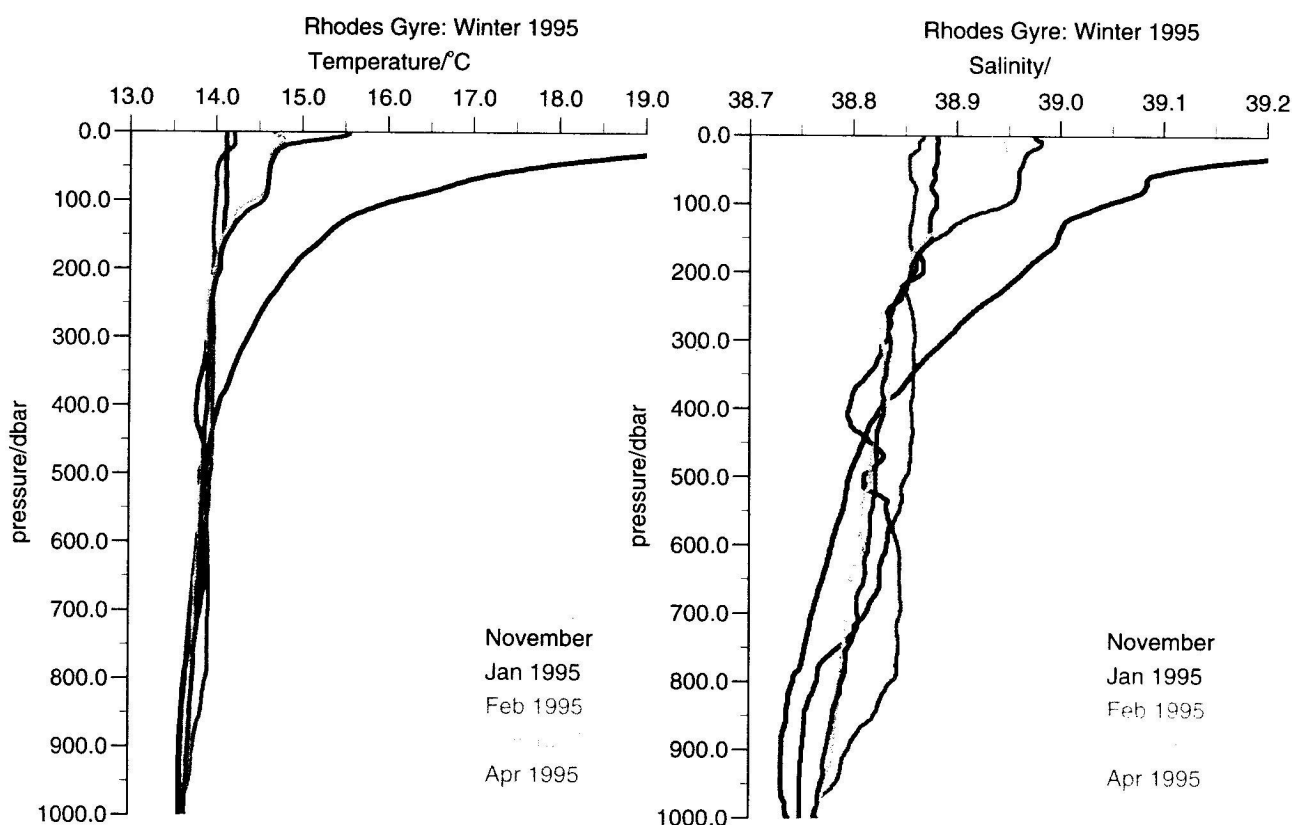
Figure 19. (left) Averaged potential temperature and (right) salinity profiles computed from the CTD stations and November climatology as shown by the different colors. See color version of this figure at back of this issue.

February. Afterward, a reversing trend started and, after mid-February, the surface buoyancy flux B_0 becomes dominantly positive. This behavior indicates that the variability of the buoyancy flux in the Rhodes Gyre is dominated by evaporation and latent heat.

[45] The buoyancy content has been computed from observations in the centre of the Rhodes Gyre during the preconditioning and postconvection phases. As in situ observations were not available at the start of the cooling events in November 1994, we use the November climatological vertical profile from selected CTD stations over the Rhodes Gyre area between 27.5°–29.5°E and 34.5°–36°N. The comparison can help to understand to what extent air-sea fluxes, occurring between the preconditioning (1 November 1994) and the first convection (30 January 1995), were responsible for the winter vertical homogenization of the water column.

[46] Figure 19 shows the averaged θ and S profiles computed from the CTD stations from the four different surveys of 1995 as well as from the November climatology calculated from historical data. These profiles show two different patterns of stratification, with the November climatology exhibiting the strongest gradients in the upper ocean. The first stratification pattern is observed in January and February during the period of strong storm events. The convective overturning and consequent homogenization of the water column extends down to 800 m, as discussed in

the previous section 4. The second stratification pattern, observed in March and April, shows an increase in temperature in the upper 150 m due to the surface heating, with salinity also increasing in the same surface layer. These temperature and salinity increases correspond to the recapping of the Rhodes chimney shown in Figure 14.

[47] The stronger upper ocean gradients in March–April are also evident in the potential density and the Brunt-Väisälä frequency (N) profiles shown in Figure 20. They have been computed from the mean temperature and salinity profiles of Figure 19, smoothed using a vertical five-point moving average to estimate the specific volume anomaly gradients. As expected, going from November to April 1995, the strong changes observed in correspondence of the shallow (≤ 50 m) maximum in the Brunt-Väisälä frequency reflect primarily the surface heating. In winter (January and February 1995) the water column is unstable from the surface to 500 m and below (not shown). However, the N profiles in November, March, and April 1995 show broad maxima in the depth range of 75–200 m because of the intrusion of the saline and much warmer Levantine Surface Water (LSW) into the gyre interior [*Malanotte-Rizzoli et al.*, 1997]. This process may occur throughout the year, as shown by the climatological profile for November.

[48] From the averaged density profiles the total buoyancy content was evaluated with respect to a reference density of 29.18 kg m^{-3} for the water depth of 50–1000 m in November
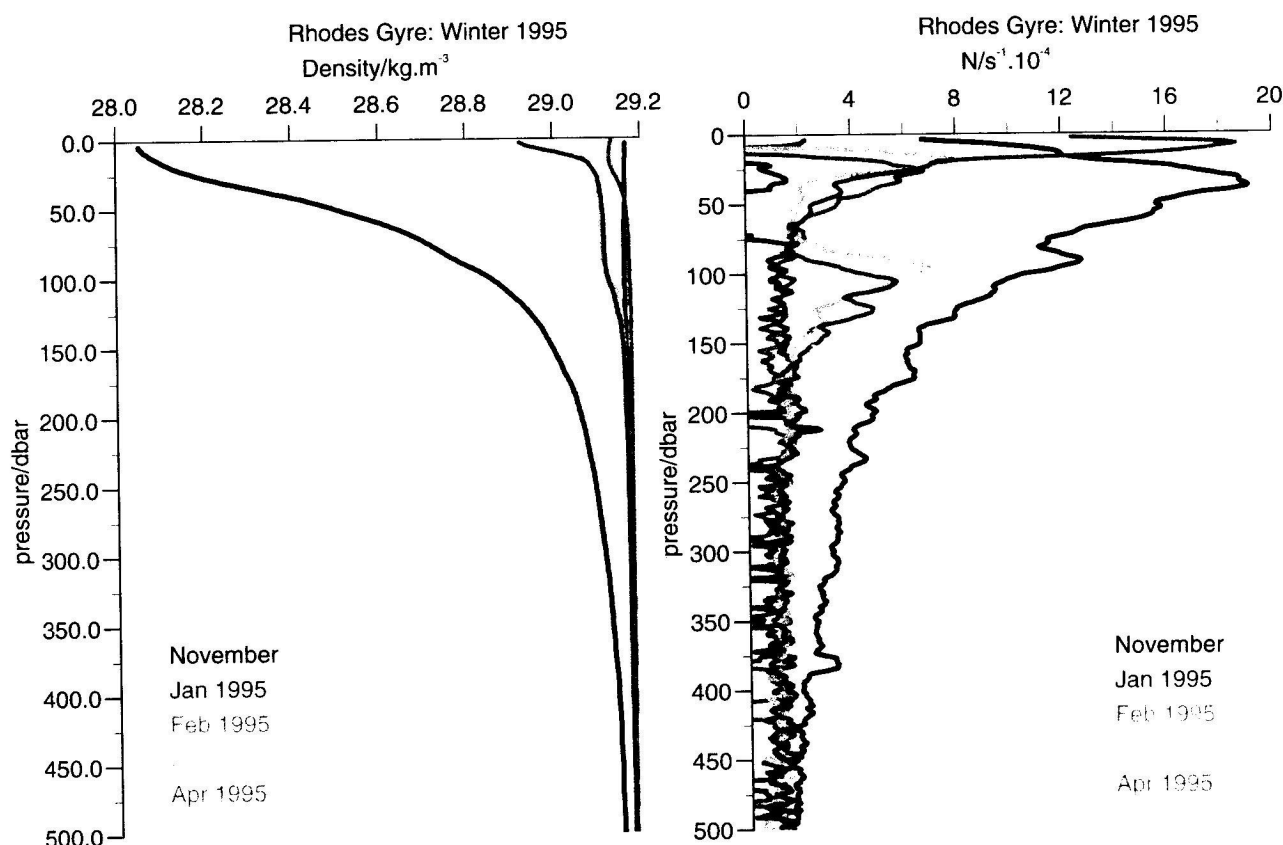
Figure 20. As in Figure 19 but for (left) the potential density and (right) the Brunt-Väisälä frequency. See color version of this figure at back of this issue.

(climatological profile), and for 30 January, 14 February, and 7 April. The upper 50 m are not considered in the computation because the wind-driven entrainment, acting at short timescales, dominates there. The wind effect is typically nonpenetrative [*Schott et al.*, 1994] and has a dissipation scale of about 50 m [*Lascaratos et al.*, 1993]. In February 1995, there is a decrease of density in the ventilated surface layer, resulting from advection of light surface water (see Figure 10) as well as from local warming in centre of the Rhodes Gyre (Figures 11 and 19). However, the buoyancy loss persists in the deepwater column through most of February 1995. Afterward, the buoyancy increases and shows the highest contrast in the upper 150 m.

[49] The evaluations of surface buoyancy flux; the initial Brunt-Väisälä frequency; the buoyancy content in the upper 1000 m of the water column; the total buoyancy change and the percentage of buoyancy change explained by surface fluxes, are given in Table 1.

[50] Table 1 shows the buoyancy content changes from November to January, from January to February, and from February to April estimated both from meteorological (B_{tot}) and CTD data (Buoyancy change). The resulting calculation shows that the first period is characterized by a loss of buoyancy of 0.612 m^2 s^{-2} if estimated from CTD or 0.491 m^2 s^{-2} if estimated from meteorological data. The buoyancy loss persists until mid-February but to a lesser extent. In the second period CTD observations registered a

buoyancy gain of 0.092 m^2 s^{-2} while meteorological measurements suggest 0.054 m^2 s^{-2}. The buoyancy content decrease in January and February is therefore well explained by the surface fluxes. During the warming period, however, the buoyancy change estimated from CTD data is almost twice the change estimated from the meteorological ones, indicating that lateral advection of light surface water toward the center of the convection region plays a significant role in increasing the vertical stability and the buoyancy content.

7. Discussion and Conclusions

[51] The last major field work of the POEM-BC program, the LIWEX experiment, was carried out in winter 1995 by the coordinated participation of the R/V of five countries. The experiment was specifically designed to observe the time evolution of the convective cyclonic chimney which is known to form in wintertime in the Rhodes Gyre of the northwestern Levantine basin. Past observational evidence has shown this chimney to be the site of wintertime LIW and/or LDW formation [*Ovchinnikov and Plakhin*, 1984; *Ozsoy et al.*, 1993; *Gertman et al*, 1994]. In this study we present a thorough analysis of the data sets collected during the three successive surveys of January, February, and March–April 1995 designed to cover the three successive phases of preconditioning, convective mixing and spreading of the newly formed water mass [*MEDOC Group*, 1970].

Table 1. Bouyancy Budget During LIWEX

Integration Period	B_{tot}, m^2 s^{-2}	N, 10^{-4} s^{-1}	Buoyancy Content, m^2 s^{-2}	Buoyancy Change, m^2 s^{-2}	% Change due to Surface Fluxes
November	/	19.14	0.686	/	/
1 November to 30 January	−0.491	1.58	0.074	−0.612	80
30 January to 14 February	−0.027	6.82	0.017	−0.057	47
14 February to 7 April	0.054	18.67	0.109	0.092	59

The major overall result of the present analysis is that the Levantine basin is a site for multiple, and different, water mass formation processes.

[52] The objective of the experiment was fully achieved, and in this study we document the "history" of the Rhodes Gyre chimney. Two further major results have emerged from the analysis. The first one is related to the dynamic structure of the upper thermocline circulation, and its possible relationship with the EMT. The second result is related to the sites of LIW formation and LIW pathways during the spreading phase. These three major results are summarized below.

7.1. LDW Chimney

[53] Winter 1995 was anomalous with respect to the climatological year in which the months of major storm events, and related strong heat losses, are February and early March. Strong outbreaks of cold, dry winds blowing from the mainland onto the northern Levantine started in fall 1994, with four episodes respectively in early and late December, mid-January and early February. These storm events were accompanied by strong total heat loss up to a maximum of 600 W m^{-2}, lasting approximately one week. These episodes were accompanied by deep convection and water mass formation, indicating that the preconditioning phase characterized by progressive reduction of static stability started as early as November 1994. The LIWEX experiment captured the last two events of mid-January and early February. Stratification was partially reestablished between these two storm episodes until the onset of spring warming in April 1995.

[54] The Rhodes Gyre chimney follows the traditional recipe of the three phases and in 1995 was the site of LDW formation, colder and denser than proper LIW. In January the survey covered the Rhodes Gyre about 10 days after the cold outbreak and a weak stratification is present in the upper 400 m. Interestingly, the signature of an earlier convective event may be present in the January profiles as they show a water mass between 400 and 800 m characterized by positive anomalies (with respect to the deep values) of temperature, salinity and oxygen, the latter one indicating a previous recent ventilation (Figure 11). The February survey mapped the gyre properties a few days after the cold outbreak, and shows the occurrence of the strong mixing phase, with the convective cell vertically homogeneous to the depth of 900 m.

[55] In April–March, recapping has occurred down to 200 m depth, with the well mixed residual core of the chimney still extending to about 800 m. Interestingly, the LDW water mass is not affected by the dynamics of the upper thermocline circulation. Mapping of properties on the LDW density horizon shows in fact that LDW does not spread away from the formation site but remains confined inside the localized Rhodes Gyre cyclonic circulation (Figure 15), possibly because of topographic effects.

[56] This observational evidence is confirmed by the evolution of surface buoyancy fluxes and buoyancy losses. The buoyancy content decrease estimated for January and February 1995 is in fact fully explained by the surface buoyancy fluxes alone. Only in the late March–April warming period lateral advection of light water from the surrounding regions becomes important, and only in the surface layer.

7.2. Circulation Dynamics

[57] The dynamic height anomaly of the surface with respect to 800 dbars of the February and the March–April surveys shows the marked difference of the upper thermocline circulation in the 1990s with respect to the 1980s (see the analysis of *Malanotte-Rizzoli et al.* [1997] for the latter decade). In 1995 the major observed featured persisted since 1991, when they were first observed [*Malanotte-Rizzoli et al.*, 1999] In the 1990s the Levantine circulation is dominated by the presence of a three-lobed strong anticyclonic area in the southern part of the basin. The three lobes are the Ierapetra and Mersah Matruha anticyclones and a third strong anticyclone in the east. The jet-like CLBC current, already captured in the February survey, separates this anticyclonic region from the northern cyclonic Rhodes Gyre. The CLBC is one of the two branches into which the MMJ bifurcates at the entrance of the Cretan Passage.

[58] This remarkable change in the 1990s of the upper thermocline circulation is most probably related to the simultaneous occurrence of the EMT, even though the coupling mechanism is not yet fully understood. A possible scenario is the following.

[59] *Samuel and Haines* [1999] and *Stratford and Haines* [2002] studied the response of the Mediterranean thermohaline circulation to the changes in the winter wind stress field , showing that the wind climatology was very different between the 1980s and the 1990s. Such changes in the surface forcing are most probably responsible for the observed changes in the wind-driven upper thermocline circulation here discussed. The presence of the three-lobed anticyclonic region in the 1990s blocks the traditional westbound pathway of LIW, which is instead veered around the anticyclonic/cyclonic structures in a local recirculation pattern. One branch of LIW is carried westward from the northern formation sites by the Asia Minor current and enters into the Aegean Sea. This LIW intrusion clearly preconditions the surface waters of the Aegean increasing their salinity above the typical values of Cretan Surface Water. If these LIW intrusions occurred continuously after 1987, under the severe storm events of successive winters increasing volumes of CIW and CDW were formed through convection. By 1991 the entire southern Aegean may have

been filled by CIW and CDW that finally spilled out from the Western Cretan Arc Straits into the Ionian interior and, at depth, into the entire abyssal Mediterranean [*Roether et al.*, 1996], thus setting about the EMT. This scenario would dynamically link the upper thermocline circulation to the occurrence of the EMT.

7.3. LIW Formation Sites and Pathways

[60] The final major result of the present study was the fortuitous observation of LIW ventilating chimneys in the January survey in the northern Levantine south of the Turkish coast. The LIW formation process does not follow the three phase process leading to LDW formation. Even in the absence of severe storm events, in fact, wind surface cooling and evaporation are sufficient to produce shallow thermostads of LIW in near-coastal areas. These shallow, well mixed chimneys can therefore be formed much more frequently in space and time than deep convective cells, hence the ubiquitous presence of LIW found in the Levantine in POEM-Phase I [*POEM Group*, 1992].The newly formed LIW subducts from the ventilated chimney on the isopycnal surfaces delimiting the chimney basis (Figure 9). Away from the region directly ventilated by the atmosphere, the spreading process is adiabatic, analogous to the subduction and along isopycnal spreading observed in the subtropical Atlantic and Pacific Oceans (WCRP CLIVAR Report 4/2001, 2001). The LIW pathways are determined by the cyclones/anticyclones of the upper thermocline circulation and were identified in the March–April survey. The first pathway shows the LIW flowing cyclonically around the Rhodes Gyre, with one branch entering the Aegean sea as discussed above. LIW is after entrained eastward by the CLBC. The second major pathway is directly southward from the formation region, and successive entrainment eastward again by the CLBC (Figure 13). Differently from LDW, LIW is therefore dynamically controlled by the upper thermocline circulation. Unfortunately, the LIWEX experiment was confined to the central Levantine and no other coastal thermostads were identified, even though some new LIW was observed in the northern rim of the Ierapetra anticyclone [*Kontoyiannis et al.*, 1999].

[61] The final major challenge is to fully understand, possibly through modeling studies in the absence of adequate observations, the dynamical mechanism responsible for the EMT and its coupling with the upper thermocline circulation that determines the LIW pathways. A possible scenario has been here suggested which needs however verification.

Appendix A

[62] The surface buoyancy flux per unit area B_0 $(m^2\ s^{-3})$ is expressed according to *Mertens and Schott* [1998] by the combination of heat and freshwater fluxes as

$$B_0 = g\left[\alpha\left(c_p\rho_o\right)^{-1}Q_t - \beta S_0(E - P)\right]$$

where g is the gravity acceleration, α is the thermal expansion coefficient, β is the expansion coefficient for salinity, S_0 is a typical surface salinity, c_p is the specific heat, $\rho_0 = 1029\ kg\ m^{-3}$ a reference seawater density, E and P the evaporation and precipitation rates.

[63] The evaporation rate E is calculated from the ratio Q_e/L_v, with $L_v = 2.45 \times 10^6\ J\ kg^{-1}$ the latent heat of evaporation. We use the meteorological data from ECMWF operational analysis, while the bulk SST values are obtained from the AVHRR satellite imagery. Precipitation data were not available and this term was set to zero. The impact of the precipitation on the surface buoyancy flux has been evaluated by *Mertens and Schott* [1998] in the case of the Gulf of Lions for winter 1992–1993 and 1993–1994. They concluded that the inclusion of precipitation into the calculation of buoyancy fluxes produces a weak reduction of 2.7% and 1.9% for the two winters examined.

[64] The total surface buoyancy flux B_{tot} over a certain time interval induces a buoyancy content change per unit area from the surface to a certain depth D. The total buoyancy content is defined with respect to a reference density σ_0, according to *Zahariev and Garrett* [1997], as

$$\int_{-D}^{0} -g\rho_0^{-1}[\rho(t,z) - \rho_0]dz = \beta(t).$$

[65] Its change can be related to the buoyancy flux by $\beta(t_2) - \beta(t_1) = B_{tot} +$ other factors. The primary contribution to the density increase results from surface buoyancy loss. The remaining factors include competing processes, like lateral advection of surface water, entrainment through the base of the water column and, in the case of a convective chimney, changes in the surface stratification (recapping) of the convective cell.
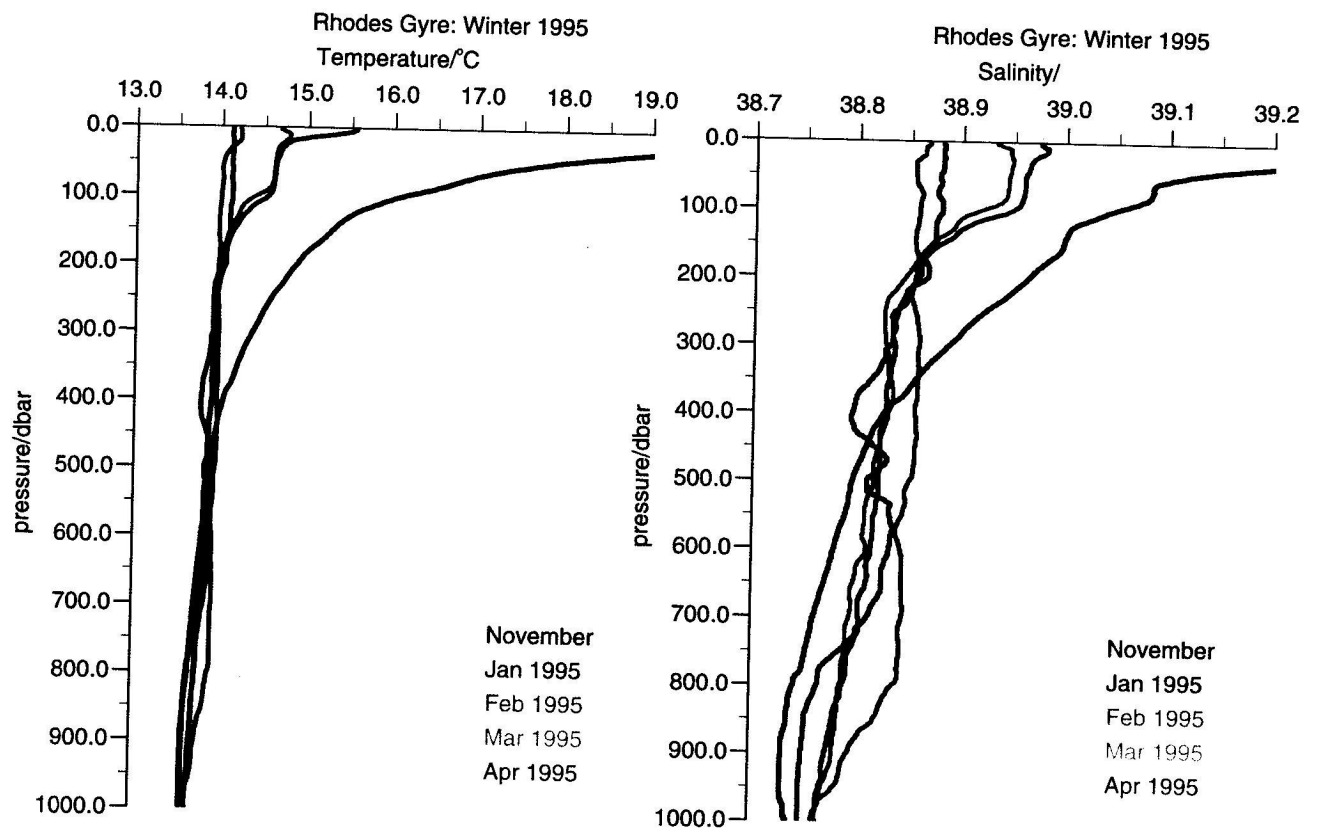
References

Castellari, S., N. Pinardi, and K. Leaman, A model study of air-sea interactions in the Mediterranean Sea, *J. Mar. Syst.*, *18*, 89–114, 1998.

Gertman, I. F., I. M. Ovchinnikov, and Y. I. Popov, Deep convection in the eastern basin of the Mediterranean Sea, *Oceanology*, *34*, 19–25, 1994.

Klein, B., W. Roether, B. B. Manca, D. Bregant, V. Beitzel, V. Kovacevic, and A. Lucchetta, The large deep water transient in the eastern Mediterranean, *Deep Sea Res., Part I*, *46*, 371–414, 1999.

Kondo, J., Air-sea bulk transfer coefficients in adiabatic conditions, *Boundary Layer Meteorol.*, *9*, 91–112, 1975.

Kontoyiannis, H., A. Theocharis, and K. Nittis, Structures and characteristics of newly formed water masses in the NW Levantine during 1986, 1992, 1995, in *The Eastern Mediterranean as A Laboratory Basin for the Assessment of Contrasting Ecosystems, NATO Sci. Ser.*, vol. 51, edited by P. Malanotte-Rizzoli and V. N. Eremeev, pp. 465–473, Kluwer Acad., Norwell, Mass., 1999.

Lascaratos, A., R. G. Williams, and E. Tragou, A mixed layer study of the formation of Levantine Intermediate Water, *J. Geophys. Res.*, *98*, 14,739–14,749, 1993.

Malanotte-Rizzoli, P., and A. R. Robinson, POEM: Physical Oceanography of the Eastern Mediterranean, *Eos Trans. AGU*, *69*(14), 194–203, 1988.

Malanotte-Rizzoli, P., et al., Experiment in the eastern Mediterranean probes the origin of deep water masses, *Eos Trans. AGU*, *77*(32), 305–307, 1996.

Malanotte-Rizzoli, P., et al., A synthesis of the Ionian Sea hydrography, circulation and water mass pathways during POEM-Phase I, *Prog. Oceanogr.*, *39*, 153–204, 1997.

Malanotte-Rizzoli, P., B. B. Manca, M. Ribera d'Alcalá, A. Theocharis, S. Brenner, G. Budillon, and E. Ozsoy, The eastern Mediterranean in the 80's and in the 90's: The big transition in the intermediate and deep circulations, *Dyn. Atmos. Oceans*, *29*, 365–395, 1999.

Manca, B. B., A. Theocharis, S. Brenner, H. Kontoyiannis, and E. Sansone, Water masses and transports between the Aegean and Levantine basins during LIWEX '95, in *The Eastern Mediterranean as a Laboratory Basin for the Assessment of Contrasting Ecosystems, NATO Sci. Ser.*, vol. 51, edited by P. Malanotte-Rizzoli and V. N. Eremeev, pp. 483–493, Kluwer Acad., Norwell, Mass., 1999.

May, P., Climatological flux estimates in the Mediterranean Sea. Part I: Winds and wind stresses, *Report 54*, 56 pp., Nav. Ocean Res. and Dev. Activ., Stennis Space Cent., Miss., 1982.

McCartney, M. S., The subtropical recirculation of mode waters, *J. Mar. Res., 40*, suppl., 427–464, 1982.

MEDOC Group, Observation of formation of deep water in the Mediterranean Sea, 1969, *Nature, 227*, 1037–1040, 1970.

Mertens, C., and F. Schott, Interannual variability of deep-water formation in the northwestern Mediterranean, *J. Phys. Oceanogr., 28*, 1410–1424, 1998.

Ovchinnikov, I. M., and E. A. Plakhin, Formation of intermediate waters of the Mediterranean Sea in the Rhodes cyclonic Gyre, *Oceanology, 23*, 960–962, 1984.

Ozsoy, E., A. Hecht, U. Unluata, S. Brenner, H. I. Sur, J. Bishop, M. A. Latif, Z. Rozentraub, and T. Oguz, A synthesis of Levantine basin circulation and hydrography 1985–1990, *Deep Sea Res., Part II, 40*, 1075–1120, 1993.

POEM Group, The general circulation of the eastern Mediterranean, *Earth Sci. Rev., 32*, 285–309, 1992.

Robinson, A. R., and P. Malanotte-Rizzoli (Eds.), Physical oceanography of the eastern Mediterranean, *Deep Sea Res., Part II, 40*, 1073–1332, 1993.

Roether, W., and R. Schlitzer, Eastern Mediterranean Deep Water renewal on the basis of chlorofluoromethane and tritium data, *Dyn. Atmos. Oceans, 15*, 333–354, 1991.

Roether, W., and R. Well, Oxygen consumption in the eastern Mediterranean, *Deep Sea Res., Part I, 38*, 1531–1551, 2001.

Roether, W., V. M. Roussenov, and R. Well, A tracer study of the thermohaline circulation of the eastern Mediterranean, in *Ocean Processes in Climate Dynamics: Global and Mediterranean Examples*, edited by P. Malanotte-Rizzoli and A. R. Robinson, pp. 371–394, Kluwer Acad., Norwell, Mass., 1994.

Roether, W., B. B. Manca, B. Klein, D. Bregant, D. Georgopoulos, V. Beitzel, V. Kovacevic, and A. Lucchetta, Recent changes in the eastern Mediterranean deep waters, *Science, 271*, 333–335, 1996.

Roether, W., B. Klein, V. Beitzel, and B. B. Manca, Property distributions and transient tracer ages in Levantine Intermediate Water in the eastern Mediterranean, *J. Mar. Syst., 18*, 71–87, 1998.

Roether, W., V. Beitzel, J. Sultenfuss, and A. Putzka, The eastern Mediterranean tritium distribution in 1987, *J. Mar. Syst., 20*, 49–61, 1999.

Samuel, S., and K. Haines, Response of the Mediterranean Sea thermohaline circulation to observed changes in the winter wind stress field in the period 1980–1993, *J. Geophys. Res., 104*, 7771–7784, 1999.

Schlitzer, R., W. Roether, M. Hausmann, H. G. Junghans, H. Oster, H. Johannsen, and A. Michelato, Chlorofluoromethane and oxygen in the eastern Mediterranean, *Deep Sea Res., 38*, 1531–1551, 1991.

Schott, F., M. Visbeck, and U. Send, Open ocean deep convection, Mediterranean and Greenland Seas, in Ocean Processes, in *Climate Dynamics: Global and Mediterranean Examples*, edited by P. Malanotte-Rizzoli and A. R. Robinson, pp. 203–225, Kluwer Acad., Norwell, Mass., 1994.

Stratford, K., and K. Haines, Modelling changes in Mediterranean thermohaline circulation 1987–1995, *J. Mar. Syst., 33–34*, 51–62, 2002.

Theocharis, A., K. Nittis, H. Kontoyiannis, E. Papageorgiou, and E. Balopoulos, Climatic changes in the Aegean Sea influence the eastern Mediterranean thermohaline circulation, *Geophys. Res. Lett., 26*, 1617–1620, 1999.

United Nations Educational, Scientific, and Cultural Organization (UNESCO), Physical Oceanography of the Eastern Mediterranean (POEM): A research programme, *UNESCO Rep. Mar. Sci., 35*, 67 pp., Paris, 1984.

United Nations Educational, Scientific, and Cultural Organization (UNESCO), Physical Oceanography of the Eastern Mediterranean (POEM): The scientific plan for the second phase of POEM, *UNESCO Rep. Mar. Sci., 57*, 27 pp., Paris, 1992.

Zahariev, K., and C. Garrett, An apparent surface buoyancy flux associated with the non linearity of the equation of state, *J. Phys. Oceanogr., 27*, 362–368, 1997.
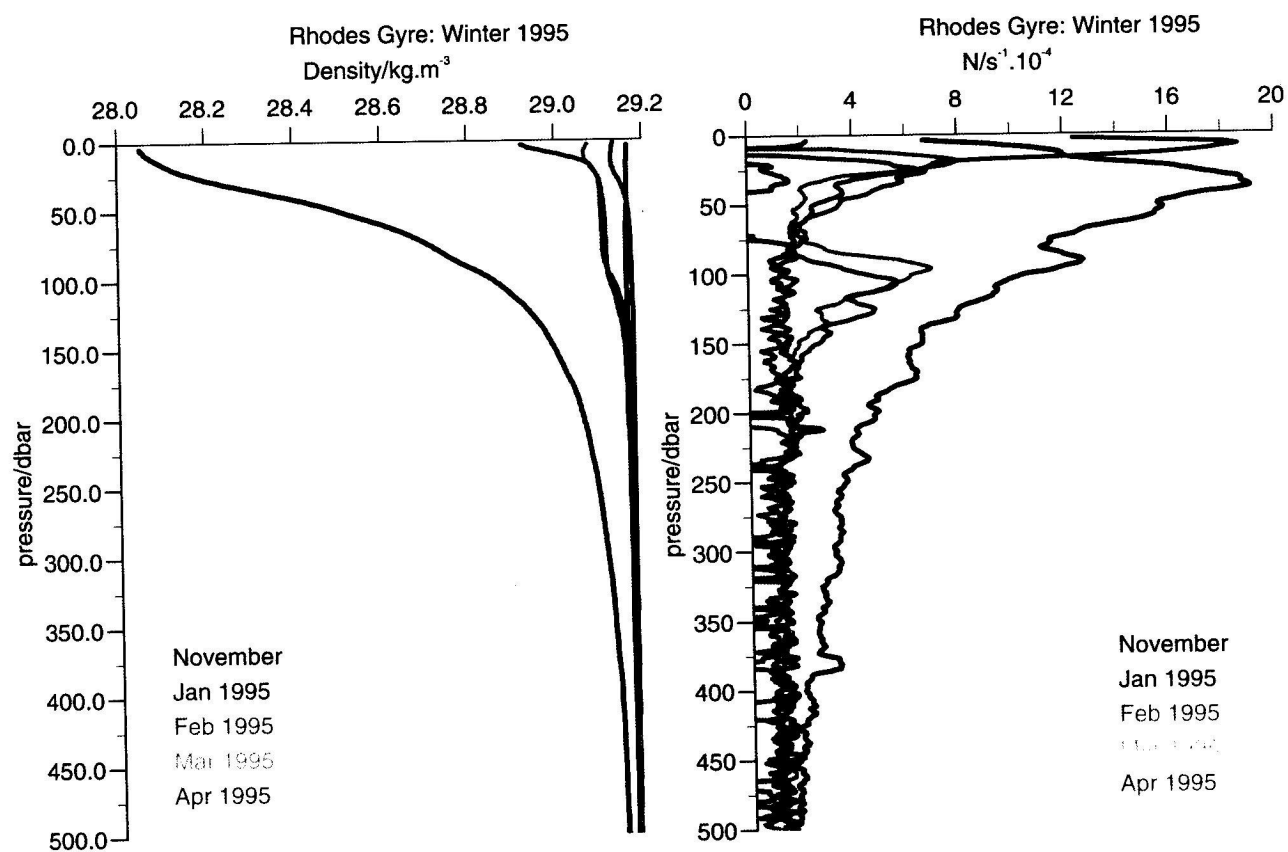
The LIWEX Group, c/o P. Malanotte-Rizzoli, Department of Earth, Atmospheric and Planetary Sciences, Massachusetts Institute of Technology, Cambridge, MA 02139, USA. (rizzoli@mit.edu)
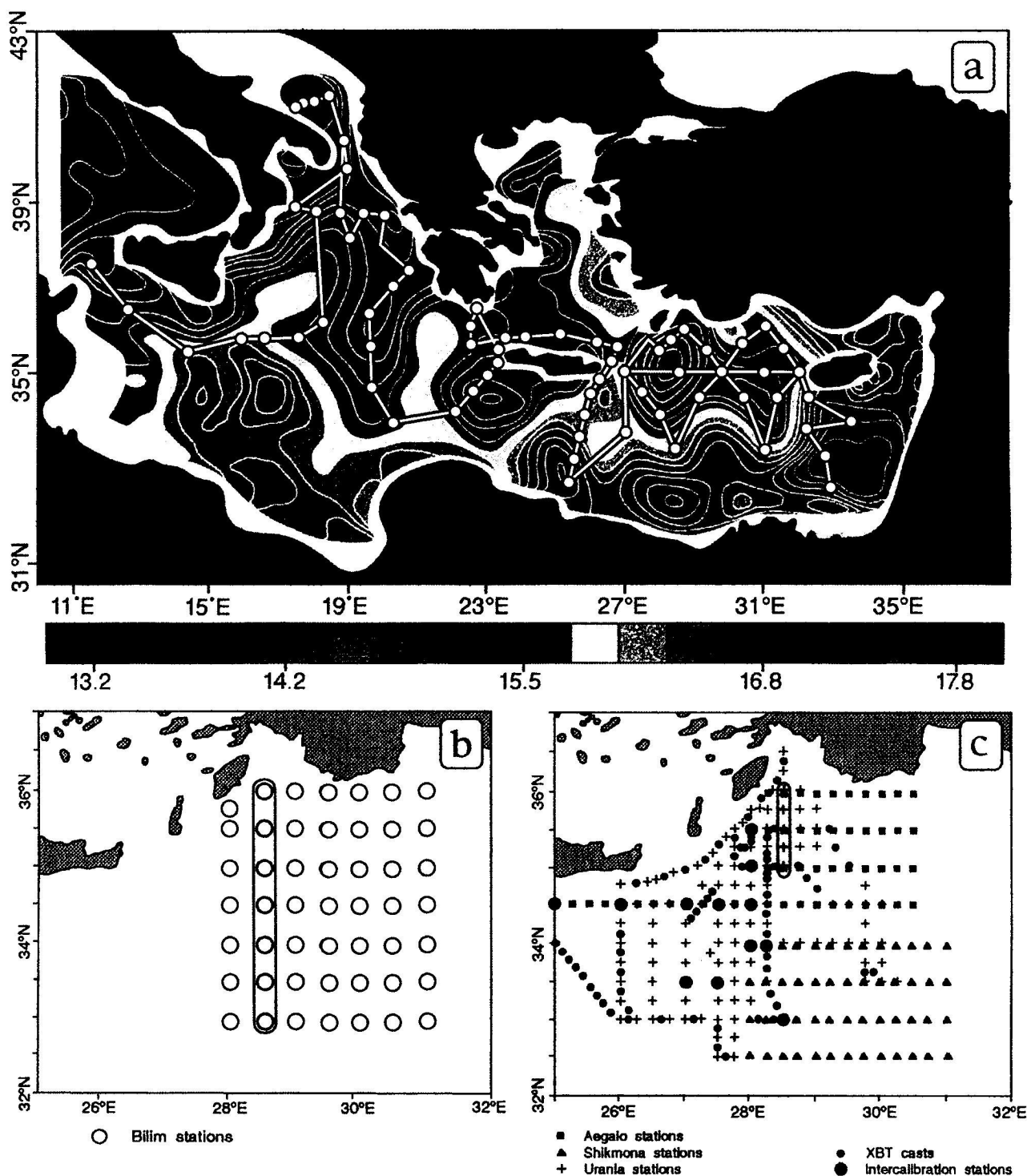
Figure 2. (a) Network of the January 1995 survey of the R/V *Meteor* (Germany) superimposed on a map of the temperature at 125 m depth. Large dots indicate hydrographic and tracer stations. (b) Network of the February 1995 survey of the R/V *Bilim* (Turkey). (c) Network of the survey of March–April 1995 carried out simultaneously by the R/Vs *Urania* (Italy), *Aegaio* (Greece), and *Shikmona* (Israel). The yellow section in Figures 2b and 2c is the one used for intercalibration.

Figure 19. (left) Averaged potential temperature and (right) salinity profiles computed from the CTD stations and November climatology as shown by the different colors.

Rhodes Gyre: Winter 1995

Density/kg.m^{-3}

Rhodes Gyre: Winter 1995

N/s^{-1}.10^{-4}

November
Jan 1995
Feb 1995
Mar 1995
Apr 1995

November
Jan 1995
Feb 1995
Mar 1995
Apr 1995

Figure 20. As in Figure 19 but for (left) the potential density and (right) the Brunt-Väisälä frequency.